# AUTS2 confers gene activation to Polycomb group proteins in the CNS

**Zhonghua Gao**[1], **Pedro Lee**[1], **James M. Stafford**[1], **Melanie von Schimmelmann**[2], **Anne Schaefer**[2], and **Danny Reinberg**[1,#]

[1]Howard Hughes Medical Institute, New York University Langone School of Medicine, Department of Biochemistry and Molecular Pharmacology, New York, NY 10016, USA

[2]Friedman Brain Institute, Department of Neuroscience, Mount Sinai School of Medicine, New York, NY 10029, USA

## Summary

Naturally occurring variations of Polycomb Repressive Complex 1 (PRC1) comprise a core assembly of Polycomb group proteins and additional factors that include, surprisingly, Autism Susceptibility Candidate 2 (AUTS2). While *AUTS2* is often disrupted in patients with neuronal disorders, the underlying mechanism is unclear. We investigated the role of AUTS2 as part of a previously identified PRC1 complex (PRC1-AUTS2), and in the context of neurodevelopment. In contrast to the canonical role of PRC1 in gene repression, PRC1-AUTS2 activates transcription. Biochemical studies demonstrated that the CK2 component of PRC1-AUTS2 thwarts PRC1 repressive activity while AUTS2-mediated recruitment of P300 leads to gene activation. ChIP-seq demonstrated that AUTS2 regulates neuronal gene expression through promoter association. Conditional targeting of *Auts2* in the mouse central nervous system (CNS) leads to various developmental defects. These findings reveal a natural means of subverting PRC1 activity, linking key epigenetic modulators with neuronal functions and diseases.

## Introduction

Polycomb group (PcG) proteins maintain repressive forms of chromatin and therefore appropriate patterns of gene repression through epigenetic mechanisms. As such, PcG proteins have key roles in normal developmental progression, stem cell biology and cancer[1–8]. The two major groups of PcG protein complexes exhibit distinct enzymatic activities: Polycomb Repressive Complex 2 (PRC2) methylates H3K27 (H3K27me)[9–12], and Polycomb Repressive Complex 1 (PRC1), catalyzes monoubiquitination of H2AK119 (H2AK119ub1)[13,14] and/or compacts chromatin[15]. There are at least six distinct groups of mammalian PRC1 complexes, PRC1.1-1.6, each comprising one of six Polycomb group RING fingers (PCGFs)[16], and the E3 ligase RING1A/B. Further diversification arises from

the mutually exclusive association of RING1A/B with either RYBP/YAF2 or one of the CBX proteins[16–18], which bind H3K27me3 through their chromodomains. Unlike their CBX-containing counterparts, RYBP-containing PRC1 complexes adopt a PRC2/ H3K27me3 independent mechanism for targeting chromatin[17].

Our previous studies revealed that PCGF3 and PCGF5 form novel PRC1 complexes comprising AUTS2[16]. *AUTS2* maps to chromosome 7q11.2, encodes a nuclear protein[19], and is frequently reported as being disrupted in individuals suffering neurological disorders, including Autism Spectrum Disorders (ASD)[20,21]. Although recent studies implicate *AUTS2* in regulating head size, neurodevelopment and enhancer function in zebrafish[22,23], the function of the AUTS2 protein has not been established nor has its role in regulating neuronal functions whose deregulation may result in pathogenesis.

The physical link between PRC1, a key epigenetic regulator, and AUTS2, a risk factor for ASD and other neurological disorders, prompted us to investigate the functional role of the AUTS2-containing PRC1 complex (PRC1-AUTS2). Here we report that PRC1-AUTS2 exhibits a novel role in transcriptional activation, in contrast to the repressive role of canonical PRC1. Furthermore, this conversion is mediated by AUTS2. Specific deletion of the *Auts2* locus in neuronal progenitor cells revealed a profound neurodevelopmental phenotype, in accordance with *AUTS2* disruptions in humans.

## Results

### An AUTS2-containing PRC1 complex

We pursued the unexpected association between PRC1 and AUTS2[16] using tandem affinity purification (TAP), followed by mass spectrometry (MS) analysis with AUTS2 fused to sequential N-terminal FLAG and HA tags (NFH). As previously reported[16], NFH-AUTS2 was associated with PCGF3, and with components of PRC1.5, including PCGF5, RING1A/B, RYBP and its homolog YAF2, and casein kinase 2 (CK2) (Fig. 1a). We focused on the AUTS2-containing PRC1.5 complex that we designated (PRC1.5-AUTS2). Interestingly, several PRC1-unrelated polypeptides, including the co-activator P300, were also associated with AUTS2 (Fig. 1a). Immunoprecipitation (IP) experiments performed with nuclear extract (NE) of 293 T-REx cells expressing a doxycycline-inducible NFH-AUTS2 and antibody against HA confirmed AUTS2 association with RING1B and PCGF5 (Fig. 1b). Other PRC1 components not associated with PRC1.5, such as CBX2, PCGF4/ BMI1, and PCGF1, comprising PRC1.2/4, PRC1.4, and PRC1.1, respectively, did not co-immunoprecipitate with AUTS2 (Fig. 1b). *Auts2* expression at the mRNA level was previously documented in mouse brain via *in situ* hybridization[19]. Indeed, RING1B, but not CBX2, interacts with AUTS2 in co-IP experiments performed using NE of E15 mouse brain and AUTS2 antibody (Fig. 1c), suggesting that PRC1.5-AUTS2 forms within the CNS.

AUTS2, PCGF5, RING1B, CK2B, and RYBP appear to form a stable complex as evidenced by glycerol gradient analysis of AUTS2-containing complexes (Fractions 9–11, Fig. 1d). Although PCGF5 bound both RING1B and AUTS2 (Fig. 1e), RING1B interacted with AUTS2 only in the presence of PCGF5 as evidenced by IPs performed *in vitro* using insect cell-expressed proteins (Fig. 1f). PCGF5 is likely required to bridge RING1B and AUTS2 in

complex formation. A similar *in vitro* IP experiment demonstrated that AUTS2 directly interacted with CK2 (Fig. 1g). Thus, PRC1.5-AUTS2 contains at least five components: RYBP/YAF2, RING1A/B, PCGF5, AUTS2, and CK2 (Fig. 1h). RING1A/B associates with PCGF5 as it does with other PCGFs[16], and recruits RYBP/YAF2. AUTS2 is incorporated through its interaction with PCGF5. Moreover, AUTS2 recruits CK2 through direct interaction.

### PRC1.5-AUTS2 activates transcription

Given that PRC1 functions as a transcriptional repressor through epigenetic mechanisms[1–3,7], we examined the effects of PRC1.5-AUTS2 on transcription and chromatin composition. We generated stable 293 T-REx cells containing an integrated luciferase reporter with five consecutive GAL4 DNA binding sites (UAS) (Fig. 2a), and one of the following doxycycline-inducible candidates: GAL4-AUTS2, GAL4-RING1B, GAL4-PCGF4, GAL4-PCGF5, or GAL4 alone. Doxycycline treatment reduced luciferase activity in GAL4-PCGF4 cells, consistent with its role in transcriptional repression (Fig. 2b). Surprisingly, doxycycline treatment dramatically increased luciferase activity in GAL4-PCGF5 or GAL4-AUTS2 cells (Fig. 2b; Extended Data Fig. 1a). This result was not due to a post-transcriptional event, as replacing the GAL4 DNA binding sequence with a FLAG-HA tag (FLAG-HA-AUTS2) resulted in the loss of AUTS2-associated transcriptional activation (Fig. 2b). Interestingly, GAL4-RING1B gave rise to considerably weaker repression, compared to GAL4-PCGF4 (Fig. 2b). Given that RING1A/B comprises all mammalian PRC1 complexes, the net outcome of GAL4-RING1B on transcription likely reflected the sum of all its associated complexes, i.e. repressive ones comprising PCGF4, and active ones comprising PCGF5 and AUTS2.

We next probed the luciferase reporter in GAL4-AUTS2 cells for the presence of PRC1.5-AUTS2 components as well as indicators of chromatin structure using chromatin IP (ChIP) experiments. Upon doxycycline induction, GAL4-AUTS2 was recruited to the promoter region of the integrated luciferase locus (Fig. 2c). As expected, RING1B and CK2B were also recruited (Fig. 2c). Consistent with the locus being transcriptionally active (Fig. 2b), Pol II was recruited, accompanied by an increase in trimethylation of histone H3 at lysine-4 (H3K4me3) that correlates with active transcription, and a reduction in trimethylation of histone H3 at lysine-27 (H3K27me3) that correlates with repression, without appreciable change in total histone H3 (Fig. 2c). Similar results were obtained using the GAL4-PCGF5 stable line, showing enrichment of Pol II and acetylation of histone H4 at lysine-16 (H4K16ac), an active histone modification, and reduction in H3K27me3 (Fig. 2d). In addition to AUTS2, GAL4-PCGF5 recruited RING1B and CK2B (Fig. 2d).

To ascertain whether reporter gene activation required other components of the PRC1.5-AUTS2 complex, we silenced RING1B or PCGF5 through siRNAs. Indeed, luciferase activity driven by GAL4-AUTS2 was reduced, relative to control siRNA treatment (Extended Data Fig. 1b, c). Similarly, *AUTS2* knockdown in GAL4-PCGF5 cells led to decreased luciferase activity (Extended Data Fig. 1d, e). Thus, PRC1.5-AUTS2 creates a chromatin environment favorable to transcription dependent upon the integrity of the complex.

## Mechanism of transcriptional activation

PRC1 can monoubiquitinate histone H2A at lysine-119 (H2AK119) through its RING1B component. Interestingly, addition of the PRC1.5-AUTS2 component, CK2, to the recombinant ternary complex RING1B-PCGF5-AUTS2 (Extended Data Fig. 2a), compromised its ability to monoubiquitinate H2AK119 (Fig. 3a). To rule out that CK2 may diminish requisite ATP levels, E1 was pre-charged with ubiquitin and then quenched by EDTA (Extended Data Fig. 2b). Inhibition of H2A monoubiquitination was still evident upon CK2 addition (Extended Data Fig. 2c). Heat inactivation of CK2 obliterated its inhibitory effect (Fig. 3b), indicating that its kinase activity may be required. Indeed, a kinase assay performed with CK2 and components used in the H2A monoubiquitination assay in the presence of $\gamma$-$^{32}$P-ATP demonstrated that CK2 phosphorylated both RING1B and UbcH5c (Extended Data Fig. 2d). An additional radiolabeled species was detectable, dependent upon the presence of nucleosomes, suggesting that CK2 may target one of the core histones under these conditions. MS analysis revealed that CK2 phosphorylated Serines 41 (S41) and 168 (S168) of RING1B (Table S1). RING1B substitution mutants were generated, containing either aspartic acid (RING1B-SD) or glutamic acid (RING1B-SE) to mimic phosphorylation at S41 and S168, respectively, or alanine (RING1B-SA) to mimic non-phosphorylated forms. Compared to the appropriate alanine substitution, RING1B-S168E was significantly weaker in H2A monoubiquitination activity, (Fig. 3c, d), while RING1B-S41D was ineffectual (Extended Data Fig. 2e). Thus, CK2 inhibits PRC1.5-AUTS2 monoubiquitination of H2AK119 through phosphorylation of RING1B at S168.

Although the presence of CK2 in PRC1.5-AUTS2 suppresses its H2A monoubiquitination activity, robust transcriptional activation likely entails an additional mechanism(s). Of note, the co-activator P300 that facilitates active transcription can associate with AUTS2 in a PRC1-independent manner (Fig. 1a). Co-IP experiments in 293T cells confirmed that AUTS2 and P300 interact and *in vitro* pull-down experiments using recombinant AUTS2 and P300 demonstrated their direct interaction (Extended Data Fig. 3). Importantly, P300 was recruited to the promoter of the luciferase reporter upon GAL4-AUTS2 induction, as evidenced by ChIP results (Fig. 4a). Moreover, RNAi-mediated silencing of P300 (Fig. 4b, insert) led to a dramatic loss in GAL4-AUTS2-mediated activation of the luciferase reporter (Fig. 4b; Extended Data Fig. 4a). A similar loss of activation was obtained upon treating the cells with C646 that specifically blocks P300 acetyltransferase activity (Fig. 4c; Extended Data Fig. 4b). Based on results using GAL4 fusions with truncated versions of AUTS2 *in vivo*, AUTS2 amino acids 404 to 913 (GAL4-AUTS2M) was sufficient to mediate transcriptional activation (Fig. 4d). Interestingly, this region overlaps a C-terminal portion of AUTS2 that correlates with more severe human phenotypes[22]. ChIP analysis revealed that truncated versions of GAL4-AUTS2 activate transcription dependent upon the ability to recruit P300 (Fig. 4e). Thus, through its recruitment of CK2 and interaction with P300, AUTS2 is key to converting repressive PRC1 to a transcriptional activator.

## AUTS2 regulates CNS gene expression

The tissue distribution of AUTS2 during development was assessed using immunohistochemistry (IHC) and validated AUTS2 antibody (Extended Data Fig. 5a). AUTS2 is highly expressed in the CNS of E15 mouse embryo, with its highest level being

apparent in the neocortex (Extended Data Fig. 5b). AUTS2 was detected in P30 adult mouse brain sections, especially in hippocampus, cerebral cortex, and Purkinje cells in the cerebellum, but at considerably lower levels (Extended Data Fig. 5c). Western blot analyses confirmed AUTS2 expression in the brain as a function of development (Extended Data Fig. 5d), consistent with reported AUTS2 mRNA levels[19]. Furthermore, AUTS2 is likely expressed primarily in neurons based on immunofluorescent analysis (Extended Data Fig. 5e) and prior studies[19].

We next performed ChIP followed by deep sequencing (ChIP-seq) to determine genomic localization of AUTS2 and RING1B, and the co-presence of various histone modifications and PolII using P1 mouse brain. AUTS2 was found predominantly in the ±5 kb region surrounding transcriptional start sites (TSS) (Extended Data Fig. 6a, b). Several promoters were co-bound by AUTS2, Pol II, and histone modifications associated with active transcription, including histone H3 acteylated at lysine-27 (H3K27ac), and H3K4me3 (Fig. 5a). Moreover, the gene bodies following these promoters were decorated with trimethylation of histone H3 at lysine-36 (H3K36me3), a modification linked with Pol II elongation (Fig. 5a). Interestingly, H3K27me3 was not detected at these AUTS2 bound promoters (Fig. 5a), consistent with the absence of detectable CBX protein in PRC1.5-AUTS2. Importantly, although RING1B was enriched at these promoters, its enzymatic product H2AK119ub1 was absent (Fig. 5a).

We then performed genome-wide analysis and identified significantly enriched peaks, as reported previously[16]. Approximately 50% of AUTS2-containing peaks comprise regions bound by H3K27ac, while only 9.0% were bound by H2AK119ub1 (Fig. 5b), consistent with the intrinsic E3 ligase activity of RING1A/B being suppressed in PRC1.5-AUTS2, as shown *in vitro* (Fig. 3a). Amongst the AUTS2 target genes identified, ~35.2% comprise the top 25% highly transcribed genes in mouse brain based on RPKM values obtained from our RNA-seq analysis in P1 mouse whole brain (Extended Data Fig. 6c). In contrast, only 8.9% comprise the bottom 25% genes with the lowest RPKM values (Extended Data Fig. 6c). We next identified genes co-targeted by AUTS2 and RING1B, and those by BMI1 and RING1B as control. Out of 4168 AUTS2 target genes, 1488 were also bound by RING1B, while out of 1919 BMI1 target genes, 1137 were also bound by RING1B. The average expression of AUTS2 or AUTS2/RING1B target genes was significantly higher than those of BMI1 or BMI1/RING1B (Fig. 5c). Of note, the overlap between AUTS2- and RING1B-targeted genes is relatively low, indicating that AUTS2 may be recruited to chromatin through PRC1-independent mechanism(s), perhaps involving other AUTS2 interacting candidates identified by our TAP analysis (Fig. 1a).

AUTS2/RING1B co-targeted loci comprised higher levels of H3K27ac and PolII, and lower levels of H2AK119ub1 and H3K27me3, relative to BMI1/RING1B co-targets (Fig. 5d). Moreover, P300 was localized to AUTS2-targeted loci and its global occupancy was higher on loci targeted by AUTS2/RING1B than those by BMI1/RING1B, as evidenced by ChIP-seq in mouse brain (Extended Data Fig. 7). Gene Ontology (GO) analysis of AUTS2 targets in mouse brain revealed enrichment of functional terms including "gene expression", "abnormality of the forebrain", and "abnormality of the cerebrum" (Fig. 5e; Table S2), indicating a role of AUTS2 in positively regulating the CNS transcription program.

RING1B was similarly associated with AUTS2 target genes in 293 T-REx cells, as evidenced by ChIP-seq (Extended Data Fig. 8). A substantial portion of HA-AUTS2 peaks (about 30%; 1664 out of 5563 peaks) was also bound by HA-RING1B (Extended Data Fig. 8c). NFH-AUTS2 induction in 293 T-REx cells was ineffectual with respect to RING1B and RYBP mRNA levels as gauged by RT-qPCR, while mRNAs levels of several genes among the top 20 HA-AUTS2 targets were generally increased (Extended Data Fig. 8f), consistent with PRC1.5-AUTS2 mediating transcriptional activation.

## Phenotypes in *Auts2* KO mice

AUTS2 function in the brain was assessed using *Auts2* conditional knockout (cKO) mice generated by crossing mice harboring loxP sites flanking exon 7 of *Auts2* with mice carrying Nestin promoter-driven Cre recombinase (Fig. 6a; Extended Data Fig. 9a, b). While *AUTS2* disruptions affect one human allele, we characterized full homozygous knockout (KO) as well as heterozygous knockout of *Auts2* (HET) to better understand the *Auts2* phenotype, as well as gene dosage effects. In humans, ~80% of all *AUTS2* disruptions are associated with either low birth weight or small stature[21]. Accordingly, we observed both a striking visual (Fig. 6a) and quantitative (Fig. 6b; Extended Data Fig. 9c) reduction in the size of the *Auts2* KO relative to wild type (WT) littermates, with HET showing an intermediate phenotype across early development. Developmental delay typically encompasses impairments in reaching normal sensorimotor, cognition and communication (e.g., speech) milestones, characteristics of the *AUTS2* phenotype[21]. We explored such developmental milestones in mice as a function of *Auts2* disruption using a pre-weanling behavioral battery including basic motor skills (e.g., righting reflex) and ultrasonic vocalizations (USVs) following maternal separation, often impaired in a variety of mouse models of neurodevelopmental disorder[24–26]. Across early development, KO mice were deficient in both righting reflex and ultrasonic vocalizations emitted (Fig. 6c, d), as well as in negative geotaxis (Extended Data Fig. 9d). While the KO showed a significantly smaller milk band at P1, early malnutrition or abnormal maternal behavior should not be fully responsible for all of the observed phenotypes, given that the HET showed phenotypes similar to the KO while having a milk band indistinguishable from WT (Extended Data Fig. 9e). While it is difficult to directly infer human pathology from mouse phenotypes, these results strongly suggest that a gene dosage-dependent disruption of mouse *Auts2* resulted in impaired developmental phenotypes characteristic of *AUTS2* disruption in humans.

Several selected genes co-targeted by AUTS2 and RING1B exhibited decreased mRNA levels in KO relative to WT mouse whole brains as evidenced by RT-qPCR (Extended Data Fig. 10). In particular, disruption of *Nat8l* has been associated with many of the phenotypes observed in *AUTS2* patients (e.g., growth delay, intellectual disability)[27–29], suggesting that *Auts2* disruption in these mice may lead to developmental defects through altered expression of its target genes.

## Discussion

Active promoters have been linked previously with the presence of PRC2 or PRC1[30–33], yet the heterogeneous compositions of these complexes hampered further investigations. Here,

we identified AUTS2 as the transformative moiety that renders PRC1 capable of transcription stimulation, through its recruitment of CK2 and P300 (Fig. 6e). These findings underscore that the natural variation in the constituents of PRC1 complexes can lead to PRC1 adopting unexpected roles in coordinating specific cellular gene expression profiles. Our findings may set a precedent for other dynamic alterations in the regulatory properties of PRC1 and perhaps PRC2, based on their constituent components.

Despite a plethora of evidence from human genetics indicating that *AUTS2* disruption is associated with neurological disorders including ASD, AUTS2 function was unclear[21]. Our results provide the first causal evidence for *Auts2* disruption leading to specific behavioral phenotypes associated with the human condition. While the precise neurobiological mechanisms underlying these developmental phenotypes are yet to be elucidated, AUTS2 association with active transcription and H3K4me3 point to its having a key role in regulating early transcriptional programs associated with normal brain development[34,35]. AUTS2 is highly enriched in the prefrontal cortex (PFC) and recent evidence suggests that the genome-wide distribution of H3K4me3 peaks fail to exhibit the normal developmental shift at a number of genes implicated in ASD pathology (e.g., PARK2, NLGN4Y, SHANK3), in the PFC of ASD patients[35]. Furthermore, recent evidence provide a strong case for aberrant epigenetic regulation in the cerebellum of ASD patients[36,37]. These findings combined with the enrichment of AUTS2 in cerebellar Purkinje cells and the PFC suggest that these brain regions may be involved in conferring the *Auts2* phenotype[26]. The novel role of AUTS2 in modulating PRC1 activity to effectively purge its repressive function and exploit the complex to attain activated transcription will likely encourage alternate directions in addressing the challenges of ASD and related neurological diseases.

## Methods

### Plasmids

For construction of pINTO-NFH-AUTS2, cDNA for human AUTS2 was purchased from ATCC and cloned into the vector pINTO-NFH carrying N-terminal FLAG and HA tags, as described previously[16]. For pINTO-GAL4-AUTS2, the same cDNA was cloned into pINTO-GAL4 with a GAL4 DNA binding sequence replacing the N-terminal FLAG and HA tags. For truncated GAL4-AUTS2, PCR was used to amplify the fragments of interest prior to inversion to the pINTO-GAL4 vector. For RING1B, PCGF4, and PCGF5, cDNA obtained from digestion of pINTO-NFH-RING1B, pINTO-NFH-PCGF4, and pINTO-NFH-PCGF5, respectively, were cloned into pINTO-GAL4. For protein expression in insect cells, cDNAs of interest were cloned into pFastbac vectors.

### Cell culture

Stable cells expressing pINTO-NFH-AUTS2 were generated from 293 T-REx cells and maintained as described previously[16]. For those expressing GAL4-fusion proteins, vector control (pINTO-GAL4) or constructs made in this vector were tranfected into 293 T-REx-luciferase cells containing a stable integrated 5XGal4RE-tk-Luc-neo construct[38], and selected with 200 μg/ml zeocin, 10 μg/ml blasticidin, and 400 μg/ml G418.

## RNA interference

Cells were transfected with siRNAs using Lipofectamine RNAiMAX (Life Technologies) according to the manufacturer's protocol. All human siRNAs were purchased: si-contr (AllStars Negative Control siRNA, cat# SI03650318) and si-RING1B(cat# SI00095543, target sequence: 5'-TGGGCTAGAGCTTGATAATAA-3') were from Qiagen; si-P300 (cat# 4392420, ID# s4695, target sequence: 5'-GGACTACCCTATCAAGTAA-3') was from Ambion; si-PCGF5 (cat# L-007089-00-0005, target sequences: 5'-CAACAACAGTGACGGAATG-3', 5'-GAGGTTGGACA ATACATTA-3', 5'-ACAAATTGCTATCTGTCTA-3', 5'-GAAGAAATTCATTCGATGT-3') and si-AUTS2 (cat# L-013932-00-0005, target sequences: 5'-TGACAGAGATAGAGATGTA-3', 5'-AGACTCATCTGTTAGTAAA-3', 5'-GAAAGGCTCAGTGATAGTT-3', 5'-CACATAA GCTGGACTTTGG-3') were from Thermo Scientific.

## Affinity purification, protein identification, and glycerol gradient

To identify proteins associated with AUTS2, tandem affinity purification was performed in nuclear extract (NE) of 293 T-REx cells expressing NFH-AUTS2, as described previously[16]. Briefly, NE prepared from $30 \times 150$ cm plates of cells was incubated with FLAG M2 beads at 4°C overnight. After 5 washes, proteins bound on the M2 beads were eluted with 500 μl FLAG peptides at 250 μg/ml at 4°C for 1 hr. The M2 eluate was then incubated with 30 μl HA beads at 4°C for 4 hr. The HA beads were washed 5 times and proteins eluted with 100 μl glycine (0.1 M, pH 2.0), and then neutralized by adding 6.5 μl Tris solution (1.5 M, pH 8.8), resulting in the final HA eluate, which was then analyzed by LC-MS.

For glycerol gradient analysis, 100 μl M2 eluate was subjected to ultracentrifugation followed by fractionation, as described previously[16]. The odd-numbered fractions were then subjected to Western blotting.

## Immunoprecipitation and *in vitro* interaction assay

Immunoprecipitation (IP) experiments were performed as described previously[16] with certain modifications. For IP, NE prepared from the indicated sources was incubated with antibodies prior to addition of protein G beads, or with FLAG or HA beads at 4°C for 3 hr. For *in vitro* interaction assay, 60 hr after infection with baculovirus for proteins of interest, Sf9 cells were harvested lysed in Lysis buffer (20 mM Tris-HCl, pH 8.0, 500 mM NaCl, 4 mM $MgCl_2$, 0.4 mM EDTA, 2 mM DTT, 20 mM β-glycerophosphate, 20 % glycerol, 0.4 mM PMSF, 1 μg/ml Pepstatin A, 1 μg/ml Leupeptin, 1 μg/ml Aprotinin), followed by centrifugation. Lysate containing indicated proteins were incubated with FLAG or HA beads at 4°C for 3hr. Beads were then washed 5 times and eluted with 100 μl glycine (0.1 M, pH 2.0), and then neutralized by adding 6.5 μl Tris solution (1.5 M, pH 8.8). The eluates were mixed with SDS sample buffer and analyzed by SDS-PAGE, followed by immunoblotting.

## Luciferase reporter assay

293T-REx-luciferase cells[38] stably transfected with pINTO-GAL4 vector control or with inserts of interest were treated with 100 ng/ml doxycycline. Cells were lysed by adding 250

μl of ice-cold lysis buffer (0.2% Triton X-100, 100 mM potassium phosphate, pH 7.8, and 1 mM DTT) and shaking for 10 min at 4°C. The cell lysate was centrifuged at 20,000$g$ for 10 min and the protein concentration of the resulting supernatant was determined by Bradford assay. 30 μg of the supernatant was assayed for luciferase activity using luciferase assay substrate (Promega).

### Purification of crosslinked nuclei from whole mouse brains

Nuclei from whole mouse brains were purified as previously described for cerebellar mouse nuclei[39] including minor changes. Briefly, CD1 pups at P1 were isolated from the embryonic sac and their whole brains quickly dissected. The whole brains were homogenized with a glass douncing homogenizer using first a loose, then tight pestle (Kimble Chase; 1984–10002). The cell homogenate was fixed with a final concentration of 1% paraformaldehyde for eight min at room temperature and the reaction quenched with 0.125 M glycine for five min at room temperature. To isolate the nuclei, the fixed homogenate was spun through a 29% iodixanol cushion and the nuclei pellet resuspended in resuspension buffer (0.25 M sucrose, 25 mM KCl, 5 mM MgCl$_2$, 20 mM Tricine, pH 7.8 and 10% Donkey Serum) supplemented with 0.15 mM spermine, 0.5 mM spermidine and EDTA-free protease inhibitor cocktail (Roche; 11836170001). Resuspended nuclei were counted using a hemocytometer and aliquots of 10$^8$ nuclei pelleted by centrifugation at 2,000 g for 15 min at 4°C. Nuclei pellets were flash-frozen in liquid nitrogen and stored at −80°C until further analysis.

### ChIP and ChIP-seq

Chromatin IP (ChIP) was performed as described previously[16]. Briefly, crosslinked and isolated nuclei were sonicated using a Diagenode Bioruptor to an average size of ~250 bp. After pre-clearing with BSA-blocked protein G Sepharose, chromatin was incubated with antibodies at 4°C overnight. The chromatin immunocomplexes were recovered with the same BSA-blocked protein G beads. For ChIP-seq library construction, 5–10 ng of DNA extracted from the chromatin immunocomplexes as described previously[15]. Libraries were prepared according to manufacturer's instructions (Illumina) and as described[15]. Immunoprecipitated DNA was first end-repaired using End-It Repair Kit (Epicenter), tailed with an A using Klenow exo minus (NEB M0212), and ligated to custom adapters with LigaFast (Promega, city, state #M8225). Fragments of 350±50 bp were size-selected and subjected to ligation-mediated PCR amplification (LM-PCR), using Phusion DNA polymerase (NEB M0530). Libraries were quantified with quantitative PCR using primers annealing to the adapter sequence and sequenced at a concentration of 7 pM on an Illumina HiSeq 2000. All sequencing data has been deposited into GEO/NCBI with the accession number GSE60411.

### ChIP-seq Analysis

ChIP-seq analysis was performed as described previously[16] with certain modifications. Sequenced reads (36bp) were aligned to the mouse reference genome (assembly mm9) for each ChIP-seq experiment in mouse brain, and to human reference genome (assembly hg19) for each ChIP-seq experiment in 293T-REx cells using Bowtie[40]. Duplicated reads were

removed with samtools[41]. ChIP-seq read density files were generated using igvtools and were viewed in Integrative Genomics Viewer (IGV)[42]. Significantly ($p<0.01$) enriched peaks for each ChIP-seq dataset were identified with QESEQ[43] and ranked according to the total number of reads mapping to them. Venn diagram of overlap among peaks (Fig. 5b; Extended Data Fig. 8c–e) was computed using the R statistical software package (http://cran.r-project.org). Correlation of AUTS2 target genes with their expression level (Extended Data Fig. 6c) was obtained by intersecting with a gene list ranked by RPKM values obtained by our RNA-seq study in P1 mouse brain. The same RPKM values were used to produce the box-and-whisker plot (Fig. 5c). ChIP reads density plots (Fig. 5d) were made using HOMER by calculating average tag densities across ±2 kb regions surrounding indicated peaks. Gene associated region annotations (Fig. 5e) were obtained with Genomic Regions Enrichment of Annotations Tool (GREAT)[44]. Genomic distribution of peaks relative to TSS (Extended Data Fig. 6b, 8b) was obtained via HOMER.

### *In vitro* H2A ubiquitination assays

Assays were performed as described previously[16] with certain modifications. Briefly, in the presence of 100 nM E1 (Boston Biochem), 500 nM UbcH5c (Boston Biochem), 10 μM HA-ubiquitin (Boston Biochem), 0.5 mM ATP, 0.1 μg/ul creatine kinase, 25 mM phosphocreatine, 1 μg/ul BSA, and 2 μl of 10× ubiquitination reaction buffer (500 mM Tris-HCl, pH 7.5, 50 mM $MgCl_2$, 10 mM DTT), reactions were assembled with reconstituted oligonucleosomes (~2.5 μg) and purified complexes or proteins in a total volume of 20 μl. After 1 hr incubation at 37°C, the reactions were stopped by boiling in SDS sample buffer, and then resolved on SDS-PAGE, followed by immunoblotting. To test the effect of CK2 (NEB) on ubiquitination (Figs. 3a and b), recombinant RING1B-PCGF5-AUTS2 complex purified from sf9 cells was incubated with CK2 in reaction buffer (20 mM Tris-HCl, pH 7.5, 50 mM KCl, and 10 mM $MgCl_2$) in the presence of ATP, creatine kinase, phosphocreatine, and BSA at 4°C for overnight to minimize the inactivation of CK2. Other components were then added and incubated for additional 1 hr at 37°C. For the experiment with E1 pre-charged with ubiquitin (Extended Data Fig. 2c), 5 time E1 was incubated with HA-ub and ATP at RT for 30 min and then quenched with 20 mM EDTA at RT for 10 min. All the other components except for nucleosomes were incubated at 4°C for overnight and also quenched by EDTA. These two mixtures were then mixed and supplemented with nuclesomes and incubated at 37°C for another 30 min.

### *In vitro* CK2 kinase assays

The reactions were assembled with components used in the *in vitro* H2A ubiquitination assays at the same concentrations, with the exception of 50 μM in the case of ATP. CK2 (NEB, P6010) was then added at 300 nM along with 2 μCi γ-^{32}P-ATP (PerkinElmer, BLU502H500UC), followed by incubation at 37°C for 30 min. The reactions were then resolved on SDS-PAGE and visualized by radiograph. For identification of phosphorylation sites on CK2 substrates, γ-^{32}P-ATP was omitted in the assays. After SDS-PAGE and Coomassie blue staining, bands corresponding to specific proteins were excised and sent for MS analysis.

## Mice

Mice harboring LoxP sites flanking Auts2 exon 7 were generated at the Janelia Farms Gene Targeting and Transgenics Resource Center and were backcrossed onto the C57Bl/6J strain. Nervous system-specific deletions of *Auts2* was performed by crossing to Nestin promoter driven Cre mice purchased from the Jackson Laboratory (stock #: 003771). After weaning, mice were housed with same sex littermates and had free access to lab chow and water. Subjects were maintained on a 12-hour light/dark cycle (lights on at 0600 h). The laboratory temperature remained at $21 \pm 1°C$. All behavioral experiments were started at $0900 \pm 1$ hrs. and performed under protocols approved by the NYU School of Medicine IACUC and in accordance with NIH "Principles of Laboratory Animal Care."

## Immunofluorescence analysis of mouse brain sections

Mouse brains were harvested at the designated time points and fixed in 4% parafolmaldehyde overnight at 4°C. The brains were then subjected to step-wise alcohol dehydration followed by tissue clearing with Histo-Clear (National Diagnostics) and embedded in paraffin (Fisher Scientific). Brains were sectioned to 16 μm and immunofluorescence was performed using the following antibodies: rabbit anti-AUTS2 (1:50, lab made), mouse anti-NeuN (1:100, Millipore, clone A60), chicken anti-GFAP (1:2000, Abcam). Slides were mounted with SlowFade (Invitrogen) and imaged in a Leica microscope.

## Developmental Phenotyping

**Testing Battery**—Mouse pups from multiple litters were used for the behavioral analysis. In this way, each datapoint represents multiple replicates (litters). The target sample size for each genotype was 8–10 as this has previously been sufficient to detect statistical differences in these behaviors, however the sample size varied due to a number of uncontrollable factors such as litter composition, subjects health, environmental confounds and statistical outliers (over 2 standard deviations from the mean). Behavior testing order was randomized for each litter of pups. Investigators were blinded to mouse genotype during behavioral testing and analysis except when the genotype was readily apparent in the phenotype (e.g., smaller stature). Total numbers of WT, HET and KO mice used in the behavioral analyses are as following (the range reflects different numbers used for each behavioral test): at P3, WT 11–17, HET 3–10, KO 6–11; at P5, WT 23–27, HET 8–13, KO 18–19; at P7, WT 7–11, HET 3, KO 8; at P9 WT 4–8, HET 2–7, KO 3. Mice harboring Cre recombinase alone did not differ from other WT littermates on any phenotype assayed thus were pooled in all analyses. Male and female mice were pooled for all analyses as no Genotype X Sex interaction was observed for any behavior measured. Behavioral tests were performed in the following order; ultrasonic vocalizations, righting reflex, negative geotaxis. Experimenters were blinded to *Auts2* genotype.

**Ultrasonic Vocalizations**—Measurement of ultrasonic vocalizations (USVs) following maternal separation was performed as reported previously[27, 45]. Briefly, at postnatal day 3, pups were isolated from their mothers. Following isolation, pups were placed in a plastic container (7cm diameter) with fresh bedding contained in a sound attenuating styrofoam

box. A condenser microphone (CM16/CMPA; Avisoft) descended ~15 cm above the pup through a hole in the top of the styrofoam box. Vocalizations were recorded with the Avisoft Recorder software (Version 4.2) using the UltraSoundGate 116Hb interface. Standard USV recording parameters were used[25]. Each recording session lasted 3 minutes. The room was maintained at $21 \pm 1°C$ during all procedures. Following generation of spectrograms, the number of USVs were counted by a trained experimenter blinded to experimental conditions with the Avisoft-SASLab Pro software.

**Righting reflex**—Righting reflex was measured by recording the latency for a pup to place all four paws on the ground after being placed on its back. Each mouse was turned over twice with average latency to right itself take between both trials.

**Negative geotaxis**—Each pup was placed on a mesh grid angled at 45° with its nose facing towards the ground. Time to turn 180° and face upwards was measured. Maximum time allowed before rescue was 30s on this task.

**Milk band measure**—At P1 the milk band was measured by visual inspection based on a standard sized milkband in a wild type C57 P1 mouse pup. Milk in the stomach was judged as either empty, 1/4, 1/2 or completely full by two independent observers with the consensus measure being used for final analysis.

**Statistics**—At each developmental timepoint, a one-way analysis of variance (ANOVA) was performed to examine the effect of genotype on each phenotype measured. Fisher's LSD was used to test hypothesized differences between genotypes. Experimental α was set 0.05.

## Extended Data

a



b



d



c



e
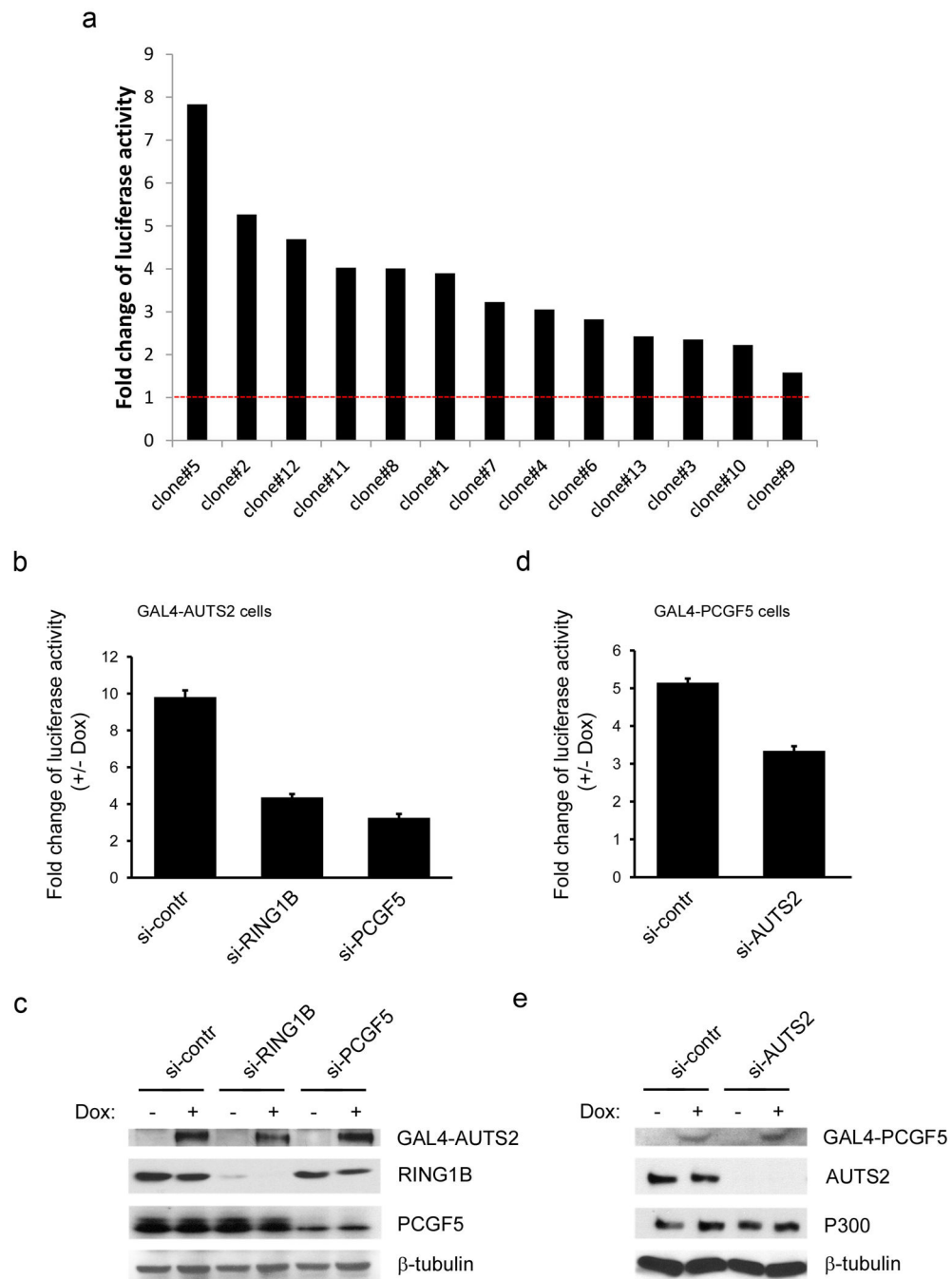


**Extended Data Figure 1.**
Requirement of the integrity of the PRC1-AUTS2 complex for transcriptional activation. **a**
Luciferase activity in screened stable cell clones expressing GAl4-PCGF5, 24 hr after
induction by doxycycline at 100 μg/ml. **b** Fold change in luciferase activity in GAl4-AUTS2
cells upon knockdown of RING1B or PCGF5. Cells were transfected with Lipofectamine
2000 RNAiMAX and siRNAs against RING1B or PCGF5, or control siRNAs for two days

and then 100 μg/ml doxycycline was added to induce GAL4-AUTS2 expression. After 24 hr after induction luciferase activity was measured. Each value is the mean of three independent measurements. Error bars represent standard error. **c** Immunoblotting of samples used for luciferase activity reporter assay as in **b** using the antibodies indicated. **d** Fold change in luciferase activity in GAl4-PCGF5 cells upon knockdown of AUTS2. Cells were treated as in **b. e** Immunoblotting of samples used for luciferase activity reporter assay as in **d** using the antibodies indicated.



E2: UbcH5c
E3: RING1B-PCGF5-AUTS2
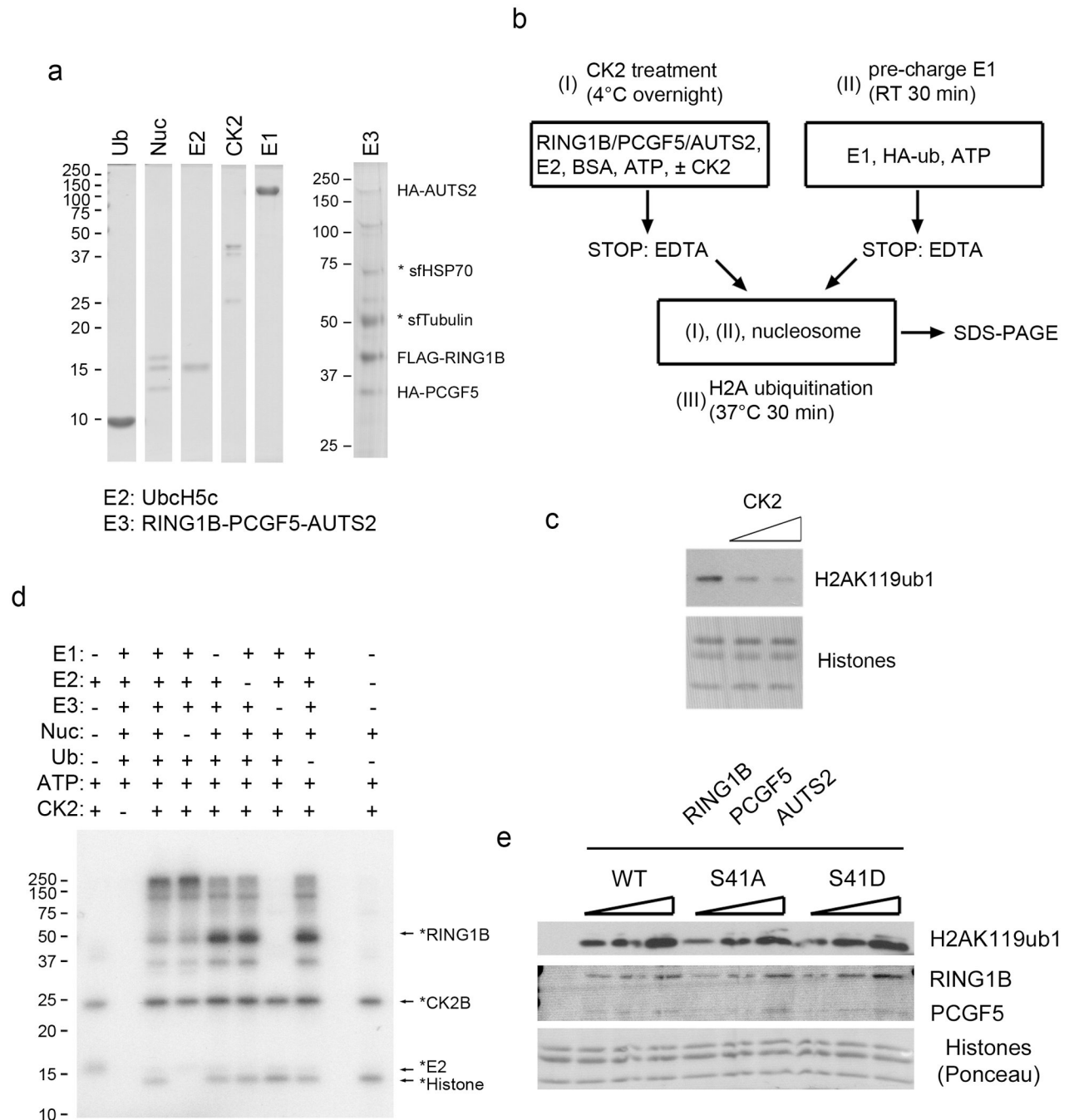
**Extended Data Figure 2.**

H2A monoubiquitination assay and CK2 kinase assay performed with γ-$^{32}$P-ATP. **a** Coomassie blue staining of factors used. **b** Scheme for H2A monoubiquitination assay with E1 that was pre-charged with HA-ubiquitin (See Methods for details). **c** Immunoblotting of H2A monoubiquitination assay as describe in **b** with increasing amounts of CK2. **d** Radiograph of CK2 kinase assay reaction products. The assay was assembled with the factors indicated, each at the same amount used in the H2A monoubiquitination assay (Methods). After incubation at 37°C for 30 min, the assay was stopped by boiling in SDS loading buffer and resolved on SDS-PAGE. Besides CK2B, which was radio-labeled presumably due to autophosphorylation, phosphorylation of RING1B and PCGF5 was detected together with a species, indicated as *histone, dependent on the presence of nucleosomes. **e** H2A monoubquitination assay performed as in Fig. 3c, using increasing amounts of RING1B-PCGF5-AUTS2 containing either RING1B-S41A (S41 to alanine), or RING1B-S41D (S41 to aspartic acid), purified from sf9 cells.
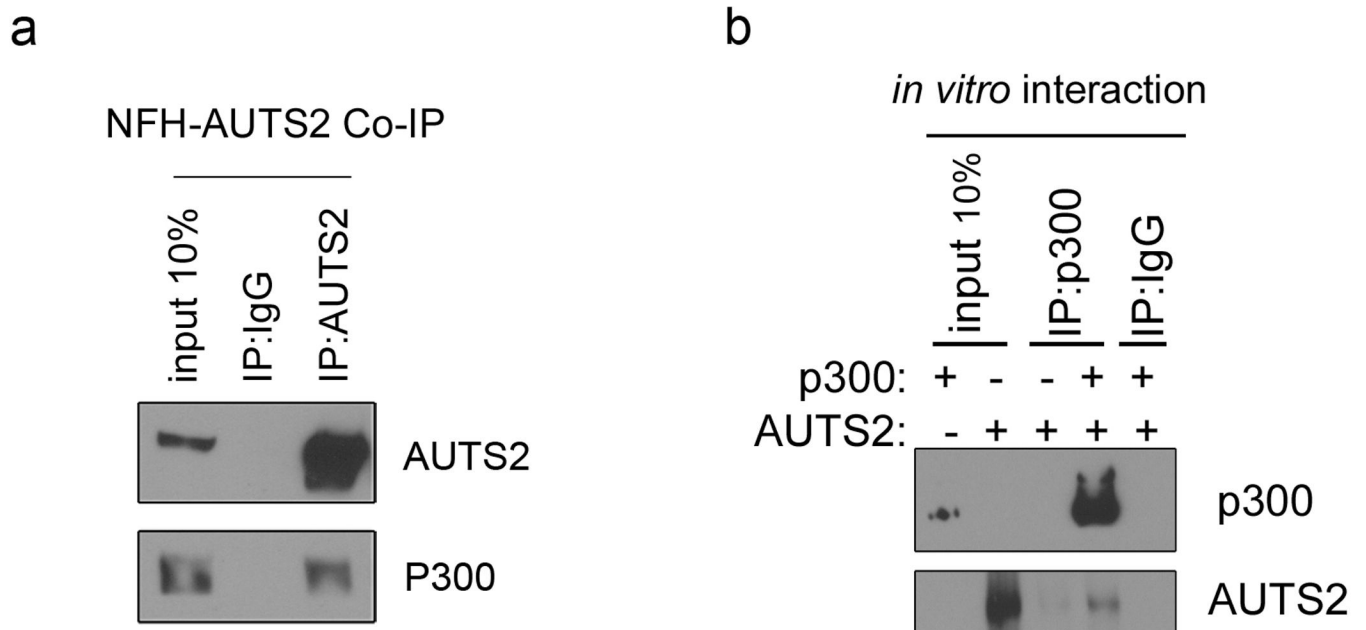


**Extended Data Figure 3.**

Interaction of AUTS2 and P300. **a** IP from NE of 293 cells expressing NFH-AUTS2 using AUTS2 antibody, followed by Western blotting for the antigens indicated. **b** IP using recombinant proteins of P300 and AUTS2 purified from Sf9 cells and a P300 antibody, followed by FLAG or HA Western blotting.

a

GAL4-AUTS2 cells



b

GAL4-AUTS2 cells
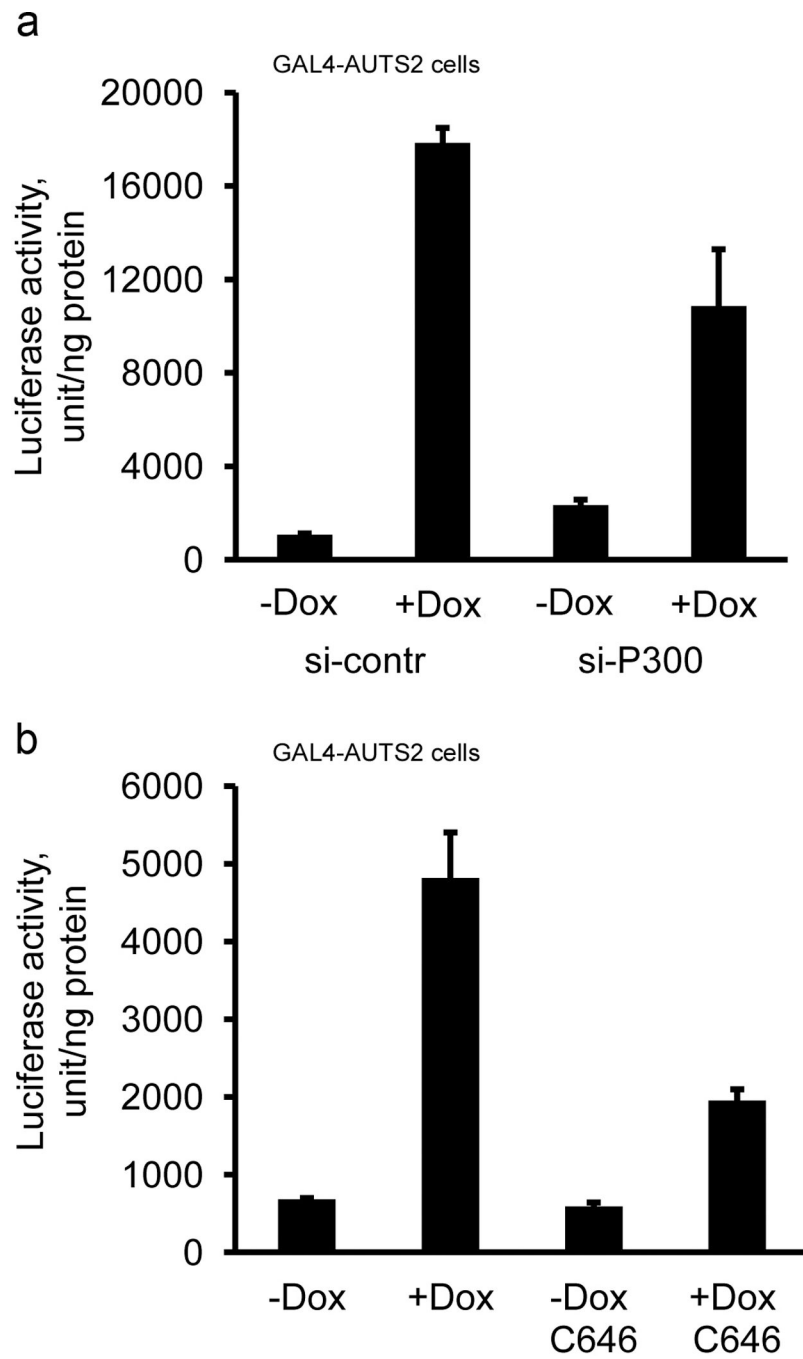


**Extended Data Figure 4.**
Luciferase activity without normalization using data from Fig. 4b and c.
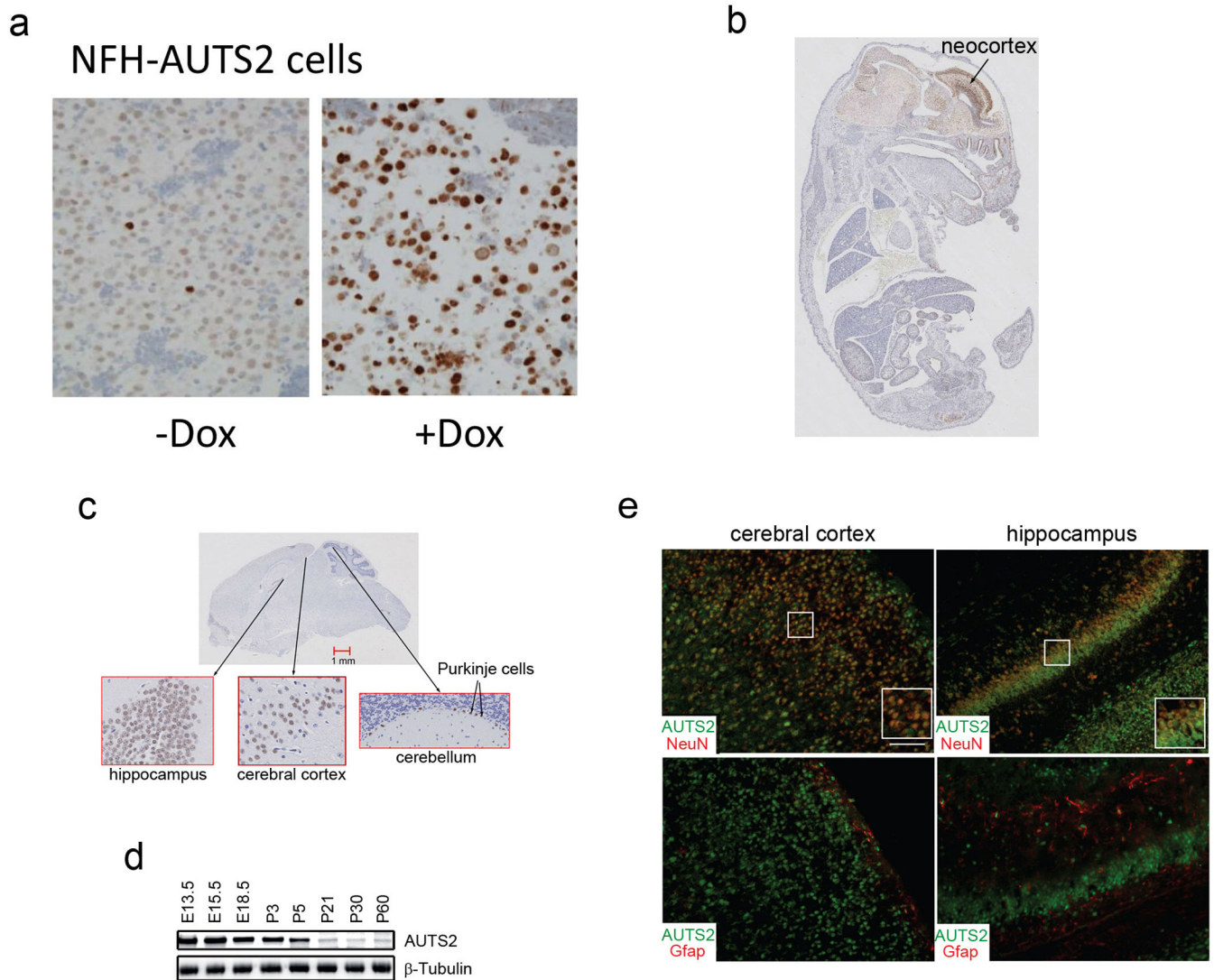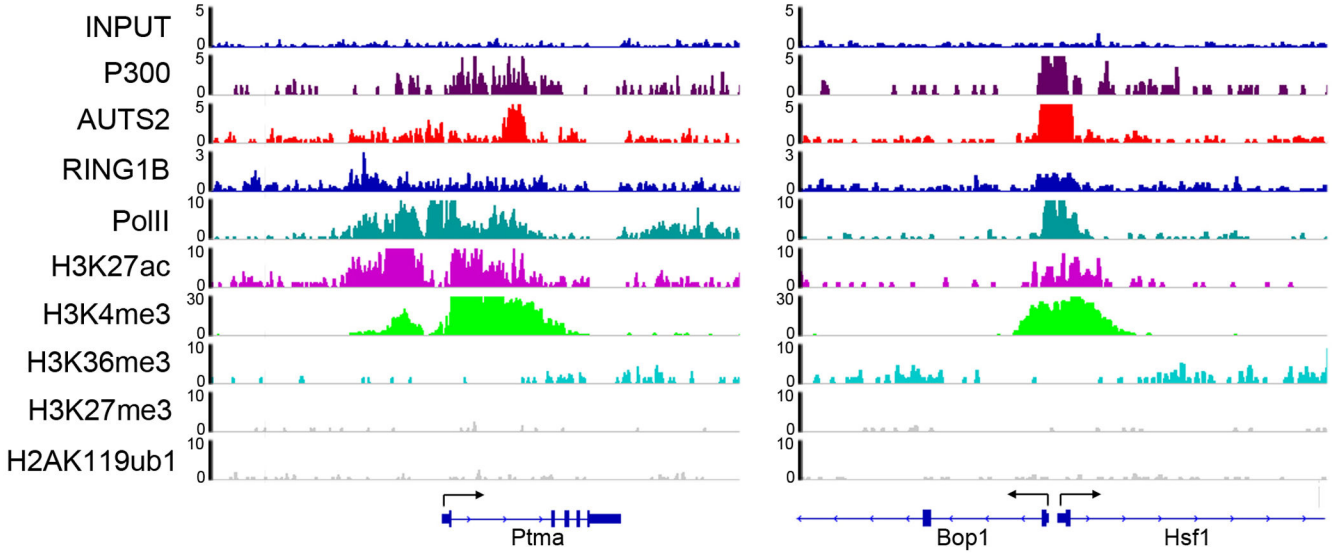
**Extended Data Figure 5.**

Expression of AUTS2 in mouse brain. **a** Validation of AUTS2 antibody by IHC in NFH-AUTS2 stable cells. Upon doxycycline induction, a stronger nuclear staining was detected compared with non-induction control, confirming the antibody we raised is suitable for IHC. **b** Detection of AUTS2 protein in a mouse embryo at E15 by immunohistochemistry (IHC) with AUTS2 antibody. **c** IHC analysis of a sagittal brain section from an adult mouse using AUTS2 antibody. **d** Expression of AUTS2 in the mouse brain. Immunoblotting was performed with whole brain extracts at various developmental stages as indicated. **e** Immunofluorescence staining of AUTS2 in P3 mouse brain. AUTS2 expression is confined to neurons (top panels) as seen by colocalization with the neuronal marker NeuN in the cortex and hippocampus. AUTS2 does not colocalize with the glial marker GFAP (bottom panels) in the same regions.

a



b



c



d
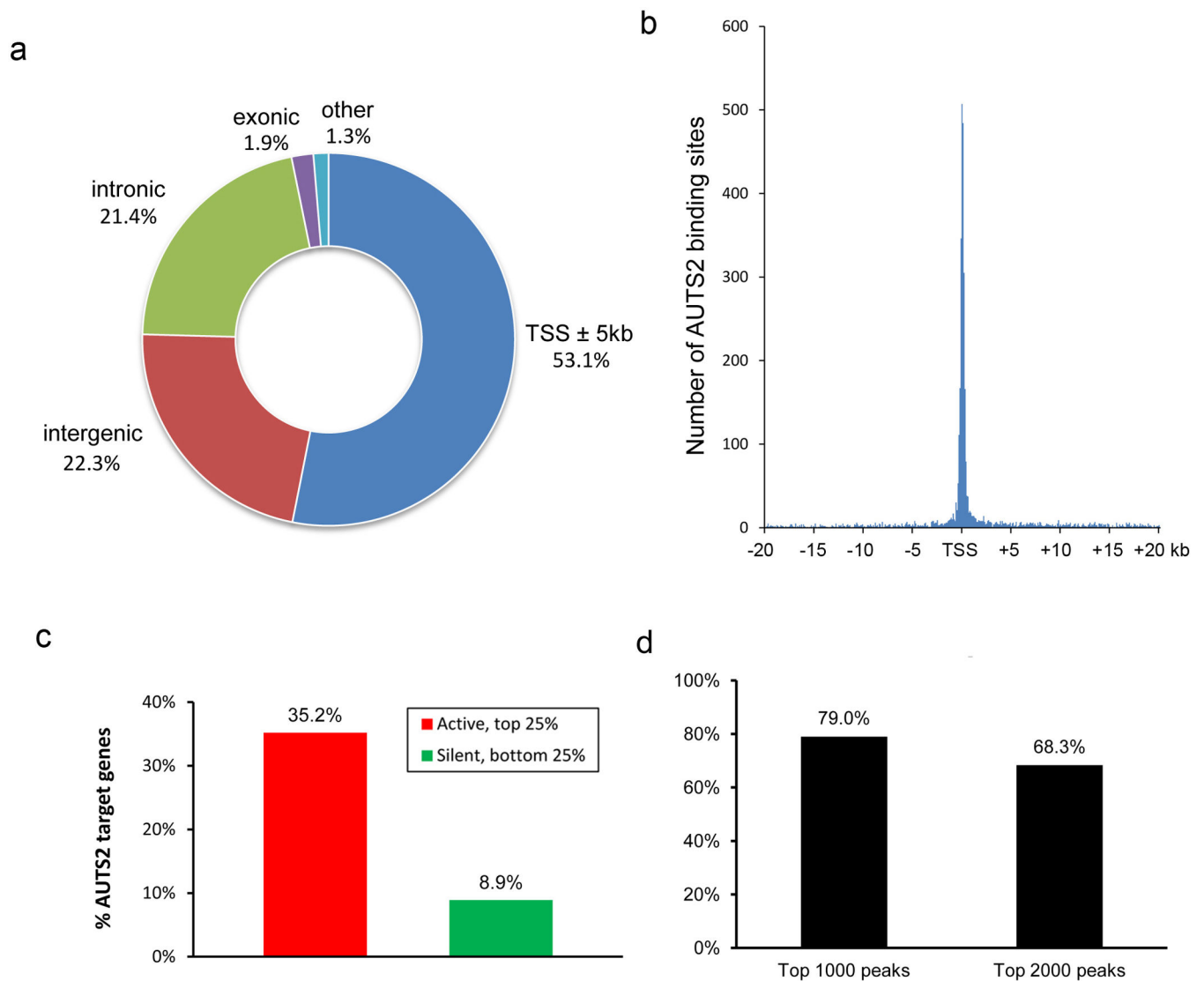


**Extended Data Figure 6.**
Genome-wide analysis of AUTS2 ChIP-seq signals. **a** HOMER was used to compute the genomic distribution of AUTS2 peaks obtained from AUTS2 ChIP-seq in mouse brain. **b** Histogram of the distribution of AUTS2 peaks relative to TSS, calculated via HOMER. **c** Percentage of AUTS2 target genes overlapped with highest (top 25%, red bar) and lowest (bottom 25%, green bar) expression levels of all genes in mouse brain. **d** Percentage of overlapped peaks between two biological replicates of AUTS2 ChIP-seq in mouse brain.

a



b
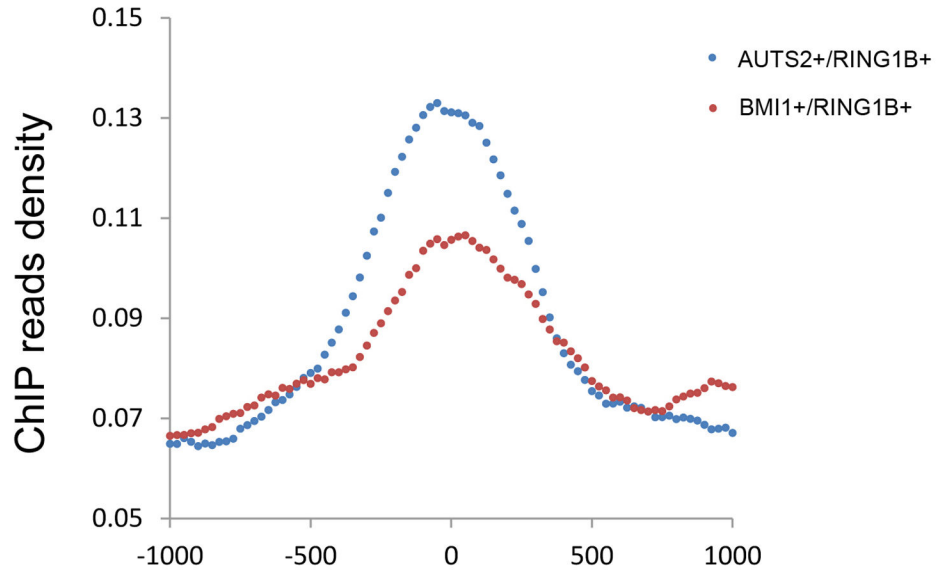


**Extended Data Figure 7.**
P300 is localized to AUTS2 targeted loci in mouse brain. **a** IGV browser views for input, P300, AUTS2, Pol II, H3K27ac, H3K4me3, H3K36me3, H3K27me3, and H2AK119ub1 ChIP-seq performed in P1 mouse brain at two representative loci. The y axis corresponds to ChIP-seq signal intensity. Gene representation at each locus is shown at the bottom. **b** ChIP reads density plots for levels of P300 at loci co-targeted by AUTS2/RING1B and BMI1/RING1B. A ±1 kb window relative to the center of peaks is shown.
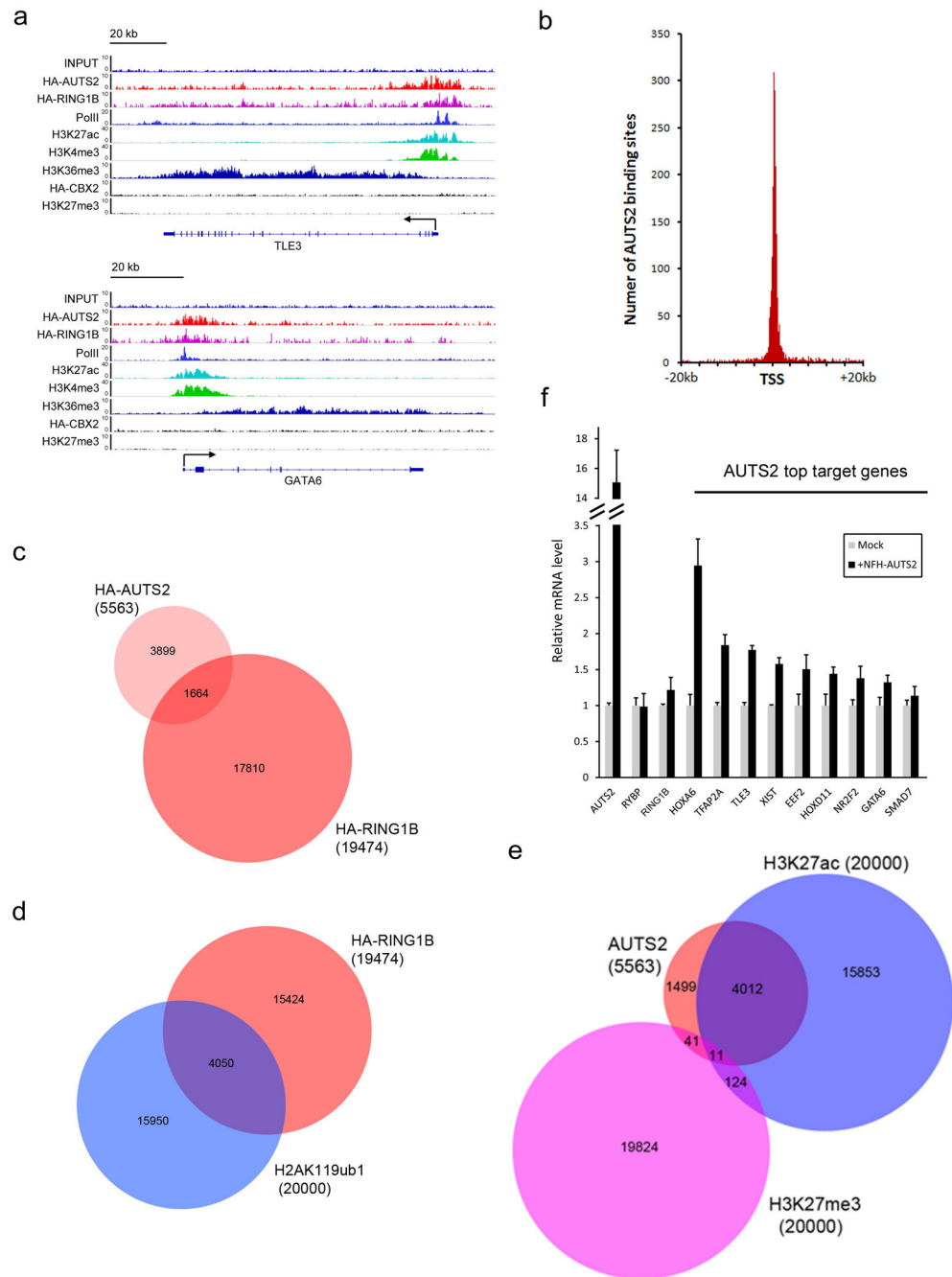
**Extended Data Figure 8.**

ChIP-seqs in 293 T-REx cells. **a** IGV browser views for input, HA-AUTS2, HA-RING1B, PolII, H3K27ac, H3K4me3, H3K36me3, HA-CBX2, and H3K27me3 ChIP-seq libraries at two representative loci. The y axis corresponds to the ChIP-seq signal intensity. Gene representation at each locus is shown at the bottom. ChIP-seq data for HA-RING1B, HA-CBX2, and H3K27me3 obtained from a previous study.[16] **b** Genomic distribution of HA-AUTS2 target regions relative to TSS. The x axis corresponds to the distance from TSS (−20 kb to +20 kb); the y axis corresponds to frequency. **c-e** Venn diagrams showing the overlap

among regions targeted by factors as indicated. **f** Analysis of mRNA levels of top targets identified by HA-AUTS2 ChIP-seq in 293 T-REx cells. RT-qPCR using the primers indicated was performed from vector control (Mock) or NFH-AUTS2 stable cell lines induced by doxycycline (+NFH-AUTS2). All values are the mean of three technical replicates and error bars represent standard deviation.
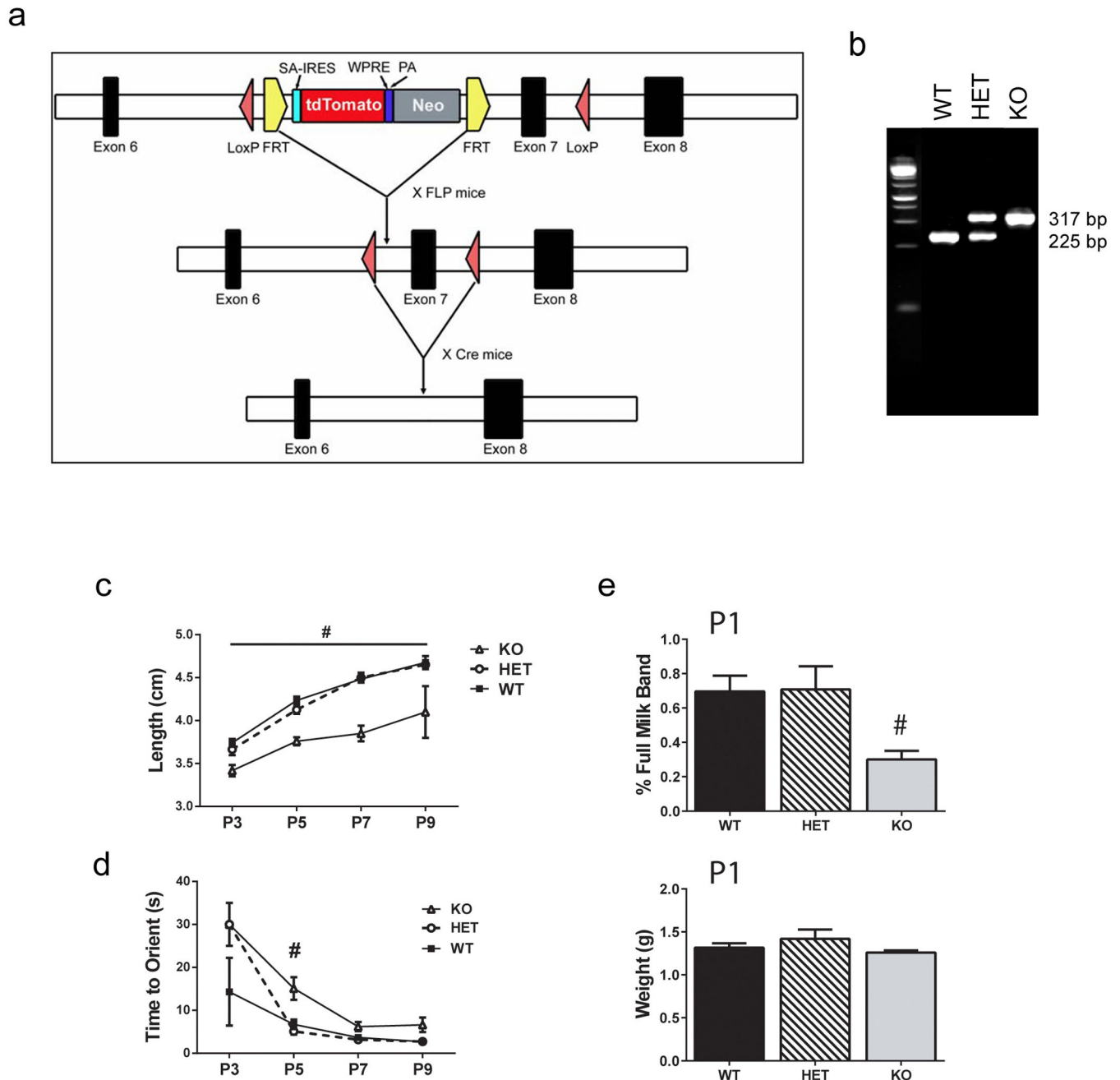


**Extended Data Figure 9.**

Generation of mice with *Auts2* conditional knockout in the nervous system and additional developmental phenotypes. **a** ES cells carrying an engineered allele of *Auts2* were generated

through homologous recombination. Specifically, two LoxP sites were placed flanking exon 7 of *Auts2*. A cassette containing SA-IRES-tdTomato and an inverted PGK-Neo (neomycin phosphotransferase gene) were flanked by two FRT (FLP recombinase target) sites and inserted between the first LoxP site and exon 7. A WPRE (woodchuck hepatitis post-transcriptional regulatory element) sequence was placed immediately downstream of tdTomato to enhance its expression. Homologous mice carrying this engineered sequence are expected to give rise to a transcript containing only the first six exons of *Auts2* followed by IRES-driven tdTomato. Red fluorescence serves as a marker for successful gene targeting. To obtain the conditional deletion of *Auts2*, these mice were crossed with FLIP mice to excise the FRT flanking sequence, resulting in floxed mice, which were then crossed with Nestin-Cre deleter mice to generate *Auts2* deletion in the nervous system. **b** Genotyping of the *Auts2* flox mice by PCR. The fast migrating species of 225 bp represents the PCR product of WT, and the species of 317 bp corresponds to the KO. **c** KO mice are significantly shorter than both HET and WT mice across development. **d** No significant difference in body weight was detected at P1, however, a significantly reduced milkb and was observed in *Auts2* KO. **e** The KO mice took significantly longer to orient their nose to an upward position. # Post-hoc difference ($p < 0.05$) between WT and KO.
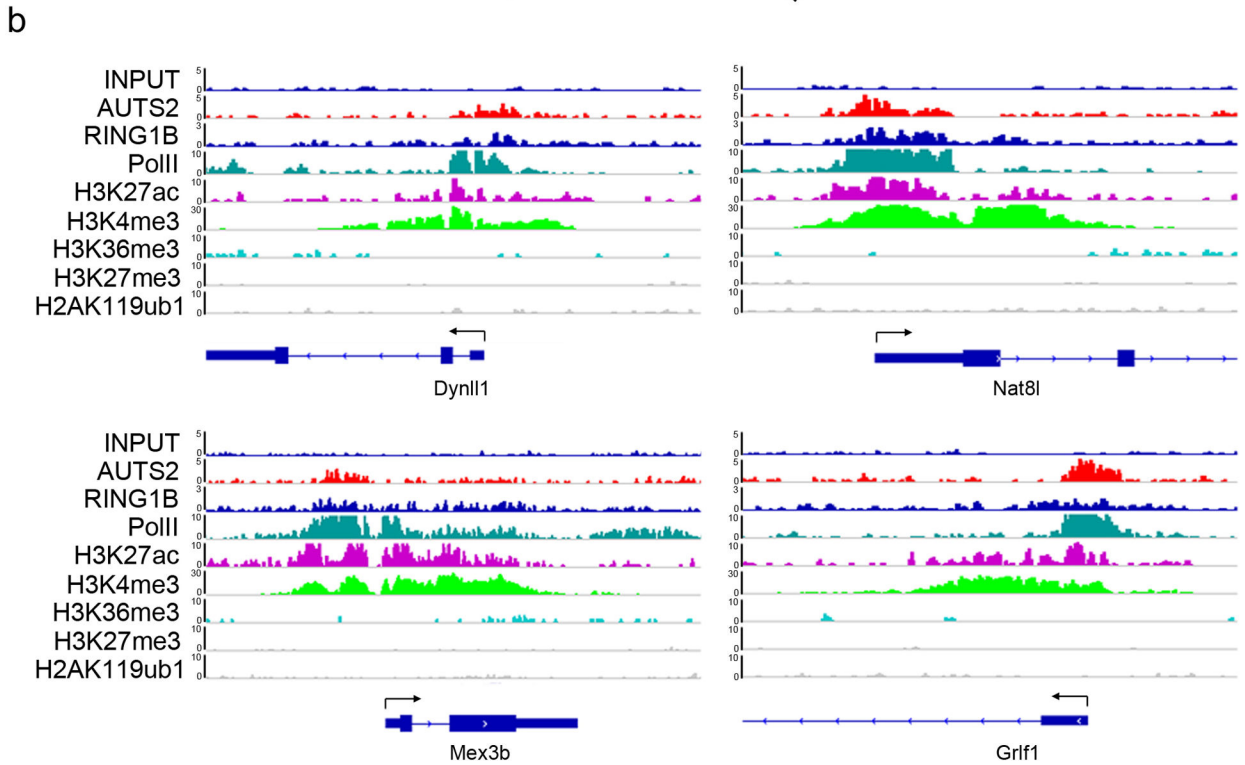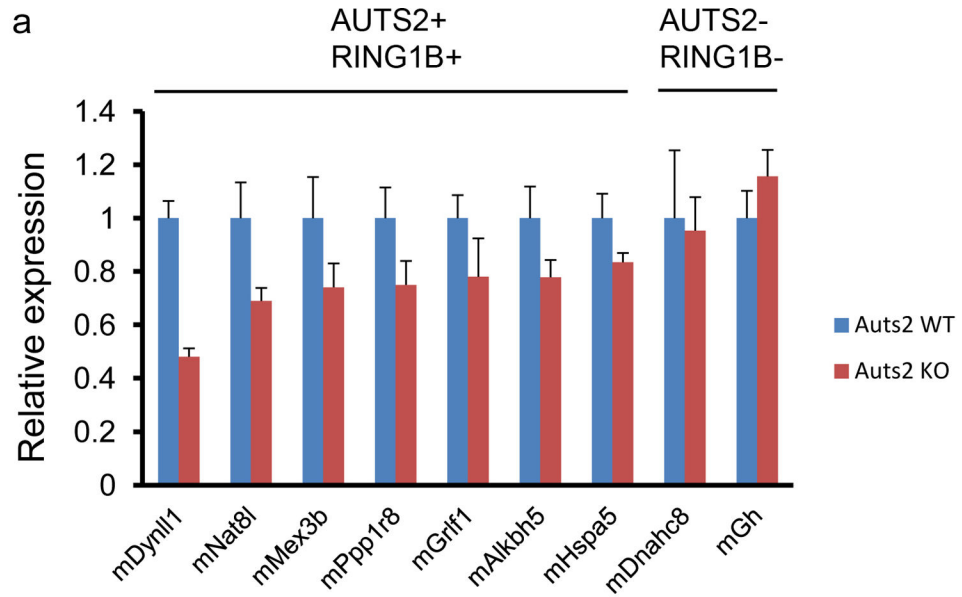
**Extended Data Figure 10.**

Altered expression of genes targeted by PRC1-AUTS2 in brains of *Auts2* KO mice. **a** Expression profiles of select genes simultaneously targeted by AUTS2 and RING1B (labeled as AUTS2+ RING1B+). As negative control, two non-target genes were used (labeled as AUTS2- RING1B-). Total RNAs were extracted from whole brains of either WT or KO mice, followed by reverse transcription to generate cDNAs for RT-qPCR. Expression levels are normalized over those in WT. All mean values of expression levels and standard errors were calculated from duplicated measurements of three biological replicates. **b** IGV

views of four representative loci for genes examined as in **a**, showing the enrichment of AUTS2, RING1B, PolII, and active histone marks.

## Supplementary Material

Refer to Web version on PubMed Central for supplementary material.

## Acknowledgements

## References

1. Simon JA, Kingston RE. Occupying chromatin: Polycomb mechanisms for getting to genomic targets, stopping transcriptional traffic, and staying put. Molecular cell. 2013; 49:808–824. [PubMed: 23473600]

2. Muller J, Verrijzer P. Biochemical mechanisms of gene regulation by polycomb group protein complexes. Current opinion in genetics & development. 2009; 19:150–158. [PubMed: 19345089]

3. Morey L, Helin K. Polycomb group protein-mediated repression of transcription. Trends Biochem Sci. 2010; 35:323–332. [PubMed: 20346678]

4. Schuettengruber B, Cavalli G. Recruitment of polycomb group complexes and their role in the dynamic regulation of cell fate choice. Development. 2009; 136:3531–3542. [PubMed: 19820181]

5. Jaenisch R, Young R. Stem cells, the molecular circuitry of pluripotency and nuclear reprogramming. Cell. 2008; 132:567–582. [PubMed: 18295576]

6. Sparmann A, van Lohuizen M. Polycomb silencers control cell fate, development and cancer. Nat Rev Cancer. 2006; 6:846–856. [PubMed: 17060944]

7. Schwartz YB, Pirrotta V. Polycomb silencing mechanisms and the management of genomic programmes. Nature reviews. Genetics. 2007; 8:9–22.

8. Margueron R, Reinberg D. The Polycomb complex PRC2 and its mark in life. Nature. 2011; 469:343–349. [PubMed: 21248841]

9. Muller J, et al. Histone methyltransferase activity of a Drosophila Polycomb group repressor complex. Cell. 2002; 111:197–208. [PubMed: 12408864]

10. Czermin B, et al. Drosophila enhancer of Zeste/ESC complexes have a histone H3 methyltransferase activity that marks chromosomal Polycomb sites. Cell. 2002; 111:185–196. [PubMed: 12408863]

11. Cao R, et al. Role of histone H3 lysine 27 methylation in Polycomb-group silencing. Science. 2002; 298:1039–1043. [PubMed: 12351676]

12. Kuzmichev A, Nishioka K, Erdjument-Bromage H, Tempst P, Reinberg D. Histone methyltransferase activity associated with a human multiprotein complex containing the Enhancer of Zeste protein. Genes Dev. 2002; 16:2893–2905. [PubMed: 12435631]

13. Wang H, et al. Role of histone H2A ubiquitination in Polycomb silencing. Nature. 2004; 431:873–878. [PubMed: 15386022]
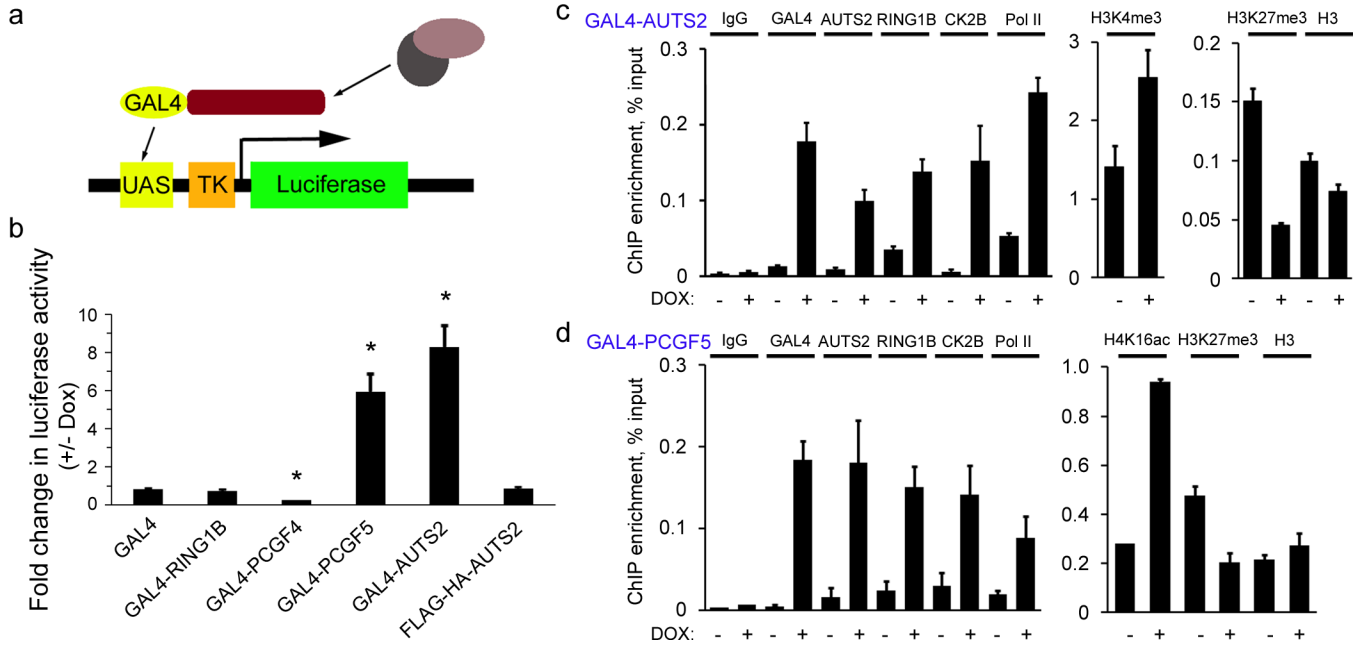
14. de Napoles M, et al. Polycomb group proteins Ring1A/B link ubiquitylation of histone H2A to heritable gene silencing and X inactivation. Dev Cell. 2004; 7:663–676. [PubMed: 15525528]

15. Francis NJ, Kingston RE, Woodcock CL. Chromatin compaction by a polycomb group protein complex. Science. 2004; 306:1574–1577. [PubMed: 15567868]

16. Gao Z, et al. PCGF homologs, CBX proteins, and RYBP define functionally distinct PRC1 family complexes. Mol Cell. 2012; 45:344–356. [PubMed: 22325352]

17. Tavares L, et al. RYBP-PRC1 Complexes Mediate H2A Ubiquitylation at Polycomb Target Sites Independently of PRC2 and H3K27me3. Cell. 2012; 148:664–678. [PubMed: 22325148]

18. Morey L, Aloia L, Cozzuto L, Benitah SA, Di Croce L. RYBP and Cbx7 Define Specific Biological Functions of Polycomb Complexes in Mouse Embryonic Stem Cells. Cell Rep. 2013; 3:60–69. [PubMed: 23273917]

19. Bedogni F, et al. Autism susceptibility candidate 2 (Auts2) encodes a nuclear protein expressed in developing brain regions implicated in autism neuropathology. Gene expression patterns : GEP. 2010; 10:9–15. [PubMed: 19948250]

20. Sultana R, et al. Identification of a novel gene on chromosome 7q11.2 interrupted by a translocation breakpoint in a pair of autistic twins. Genomics. 2002; 80:129–134. [PubMed: 12160723]

21. Oksenberg N, Ahituv N. The role of AUTS2 in neurodevelopment and human evolution. Trends in genetics : TIG. 2013; 29:600–608. [PubMed: 24008202]

22. Beunders G, et al. Exonic deletions in AUTS2 cause a syndromic form of intellectual disability and suggest a critical role for the C terminus. American journal of human genetics. 2013; 92:210–220. [PubMed: 23332918]

23. Oksenberg N, Stevison L, Wall JD, Ahituv N. Function and Regulation of AUTS2, a Gene Implicated in Autism and Human Evolution. Plos Genet. 2013; 9

24. Scattoni ML, Gandhy SU, Ricceri L, Crawley JN. Unusual repertoire of vocalizations in the BTBR T+tf/J mouse model of autism. PloS one. 2008; 3:e3067. [PubMed: 18728777]

25. Scattoni ML, Crawley J, Ricceri L. Ultrasonic vocalizations: a tool for behavioural phenotyping of mouse models of neurodevelopmental disorders. Neuroscience and biobehavioral reviews. 2009; 33:508–515. [PubMed: 18771687]

26. Fujita E, et al. Ultrasonic vocalization impairment of Foxp2 (R552H) knockin mice related to speech-language disorder and abnormality of Purkinje cells. Proc Natl Acad Sci U S A. 2008; 105:3117–3122. [PubMed: 18287060]

27. Wiame E, et al. Molecular identification of aspartate N-acetyltransferase and its mutation in hypoacetylaspartia. The Biochemical journal. 2010; 425:127–136. [PubMed: 19807691]

28. Boltshauser E, et al. Follow-up of a child with hypoacetylaspartia. Neuropediatrics. 2004; 35:255–258. [PubMed: 15328569]

29. Furukawa-Hibi Y, et al. Absence of SHATI/Nat8l reduces social interaction in mice. Neuroscience letters. 2012; 526:79–84. [PubMed: 22940080]

30. Kondo T, et al. Polycomb Potentiates Meis2 Activation in Midbrain by Mediating Interaction of the Promoter with a Tissue-Specific Enhancer. Developmental Cell. 2014; 28:94–101. [PubMed: 24374176]

31. Mousavi K, Zare H, Wang AH, Sartorelli V. Polycomb protein Ezh1 promotes RNA polymerase II elongation. Mol Cell. 2012; 45:255–262. [PubMed: 22196887]

32. Yu M, et al. Direct recruitment of polycomb repressive complex 1 to chromatin by core binding transcription factors. Mol Cell. 2012; 45:330–343. [PubMed: 22325351]

33. Frangini A, et al. The Aurora B Kinase and the Polycomb Protein Ring1B Combine to Regulate Active Promoters in Quiescent Lymphocytes. Mol Cell. 2013; 51:647–661. [PubMed: 24034696]

34. Cheung I, et al. Developmental regulation and individual differences of neuronal H3K4me3 epigenomes in the prefrontal cortex. Proc Natl Acad Sci U S A. 2010; 107:8824–8829. [PubMed: 20421462]

35. Shulha HP, Cheung I, Guo Y, Akbarian S, Weng Z. Coordinated cell type-specific epigenetic remodeling in prefrontal cortex begins before birth and continues into early adulthood. PLoS Genet. 2013; 9:e1003433. [PubMed: 23593028]

36. James SJ, Shpyleva S, Melnyk S, Pavliv O, Pogribny IP. Complex epigenetic regulation of engrailed-2 (EN-2) homeobox gene in the autism cerebellum. Translational psychiatry. 2013; 3:e232. [PubMed: 23423141]

37. Ladd-Acosta C, et al. Common DNA methylation alterations in multiple brain regions in autism. Molecular psychiatry. 2013

## References (For Methods)

38. Vaquero A, et al. Human SirT1 interacts with histone H1 and promotes formation of facultative heterochromatin. Mol Cell. 2004; 16:93–105. [PubMed: 15469825]

39. Kriaucionis S, Heintz N. The nuclear DNA base 5-hydroxymethylcytosine is present in Purkinje neurons and the brain. Science. 2009; 324:929–930. [PubMed: 19372393]

40. Langmead B, Trapnell C, Pop M, Salzberg SL. Ultrafast and memory-efficient alignment of short DNA sequences to the human genome. Genome Biol. 2009; 10

41. Li H, et al. The Sequence Alignment/Map format and SAMtools. Bioinformatics. 2009; 25:2078–2079. [PubMed: 19505943]

42. Robinson JT, et al. Integrative genomics viewer. Nat Biotechnol. 2011; 29:24–26. [PubMed: 21221095]

43. Asp P, et al. Genome-wide remodeling of the epigenetic landscape during myogenic differentiation. P Natl Acad Sci USA. 2011; 108:E149–E158.

44. McLean CY, et al. GREAT improves functional interpretation of cis-regulatory regions. Nat Biotechnol. 2010; 28:495–U155. [PubMed: 20436461]

45. Hofer MA, Shair HN, Brunelli SA. Ultrasonic vocalizations in rat and mouse pups. Current protocols in neuroscience / editorial board, Jacqueline N. Crawley … [et al.]. 2002 Chapter 8, Unit 8 14.

**Figure 1. Characterization of the PRC1.5-AUTS2 complex**

**a** Heat map of PCGF5- and AUTS2-associated polypeptides. Sequential FLAG and HA affinity purification (TAP) followed by liquid chromatography-mass spectrometry (LC-MS) (Methods) was performed in inducible 293T-REx cells expressing FLAG-HA-tagged bait proteins (PCGF5 TAP from an earlier report)[16] indicated at the top. The spectrum count of each protein is color-coded and displayed as a heat map.

**b** Immunoprecipitation (IP) from nuclear extract (NE) of NFH-AUTS2 cells in the absence or presence of doxycycline at 100 μg/ml, using HA beads. Bound proteins were resolved on SDS-PAGE and detected by Western blotting for the antigens indicated. 5% of input was loaded in all cases, unless indicated otherwise.

**c** IP from NE of mouse brain using AUTS2 antibody, followed by Western blotting for the antigens indicated.

**d** Glycerol gradient (15–35%) analysis of FLAG-purified NFH-AUTS2 complexes. Every other fraction was resolved on SDS-PAGE followed by immunoblotting for the antigens indicated.

**e – g** IP with lysates from Sf9 cells expressing the proteins indicated, using HA (**e**) or FLAG beads (**f** and **g**), followed by Western blotting using FLAG or HA antibodies.

**h** Schematic organization of PRC1.5-AUTS2. See text for details.

**Figure 2. Impact of AUTS2 on chromatin architecture and transcription**

**a** Schematic of the luciferase reporter system.

**b** Fold change in luciferase activity in cells expressing GAl4, GAl4-RING1B, GAl4-PCGF4, GAl4-PCGF5, GAl4-AUTS2, and FLAG-HA-AUTS2, after 24 hr doxycycline (100 μg/ml) induction. In this and subsequent luciferase reporter assays, each value is the mean of three independent measurements with error bars representing standard error. * indicates $p<0.05$ by two-sided $t$-test, compared with GAL4 control.

**c – d** ChIP using the antibodies indicated and GAl4-AUTS2 and GAl4-PCGF5 cells, respectively, before and after doxycycline induction. ChIP enrichment is expressed as percentage of input. All center values represent the average of three technical replicates with error bars indicating standard deviation in this and all other ChIP experiments ELSEWHERE IN THE ARTICLE.
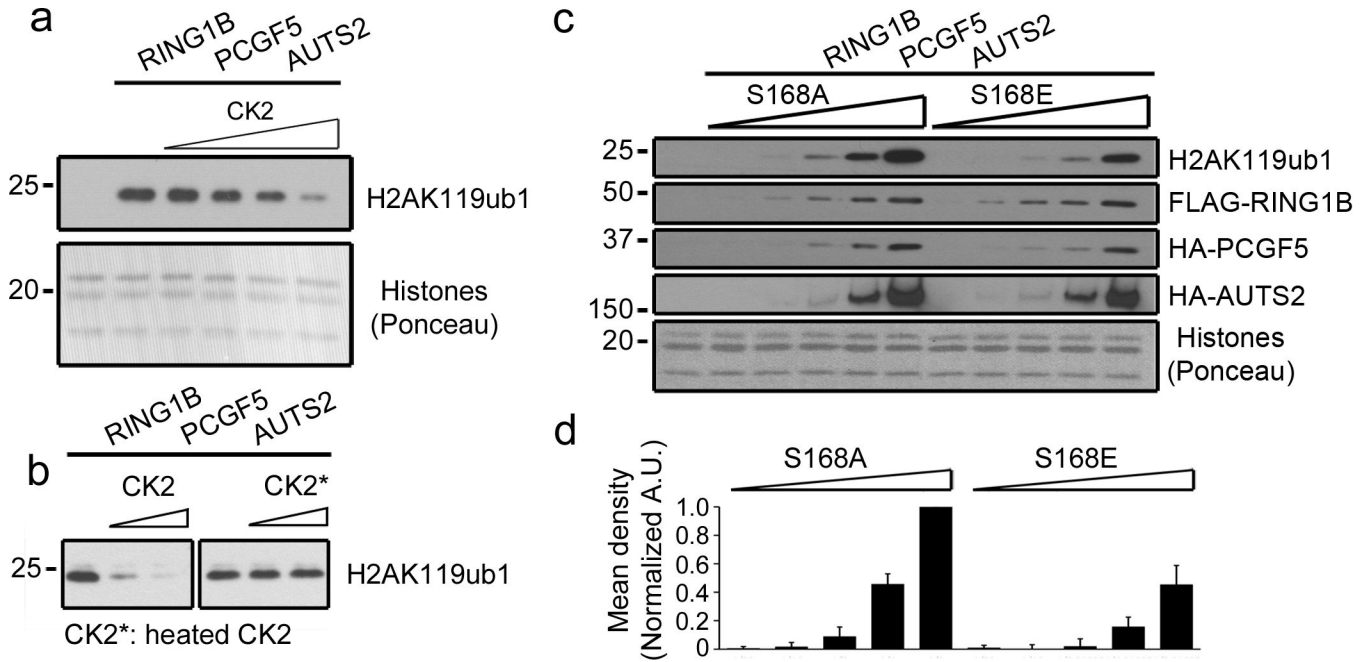
**Figure 3. CK2 inhibits H2A monoubiquitination activity of PRC1.5-AUTS2**

**a** *In vitro* nucleosomal H2A monoubquitination assay using RING1B-PCGF5-AUTS2 expressed in and purified from Sf9 cells (Methods), as a function of the presence of recombinant CK2. Reaction products were resolved on SDS-PAGE, followed by immunoblotting for H2AK119ub1. Ponceau staining of histones is shown (bottom).

**b** Effect of heat-treatment of CK2 at 95°C for 15 min prior to addition to the H2A monoubquitination assay performed as in **a**.

**c** H2A monoubquitination assay (Methods) using increasing amounts of RING1B-PCGF5-AUTS2 containing either RING1B-S168A (S168 to alanine), or RING1B-S168E (S168 to glutamic acid), purified from sf9 cells.

**d** Densitometry of H2A monoubquitination based on three independent experiments as in **c**. Quantification was done by using Image J. Error bars represent standard deviation.
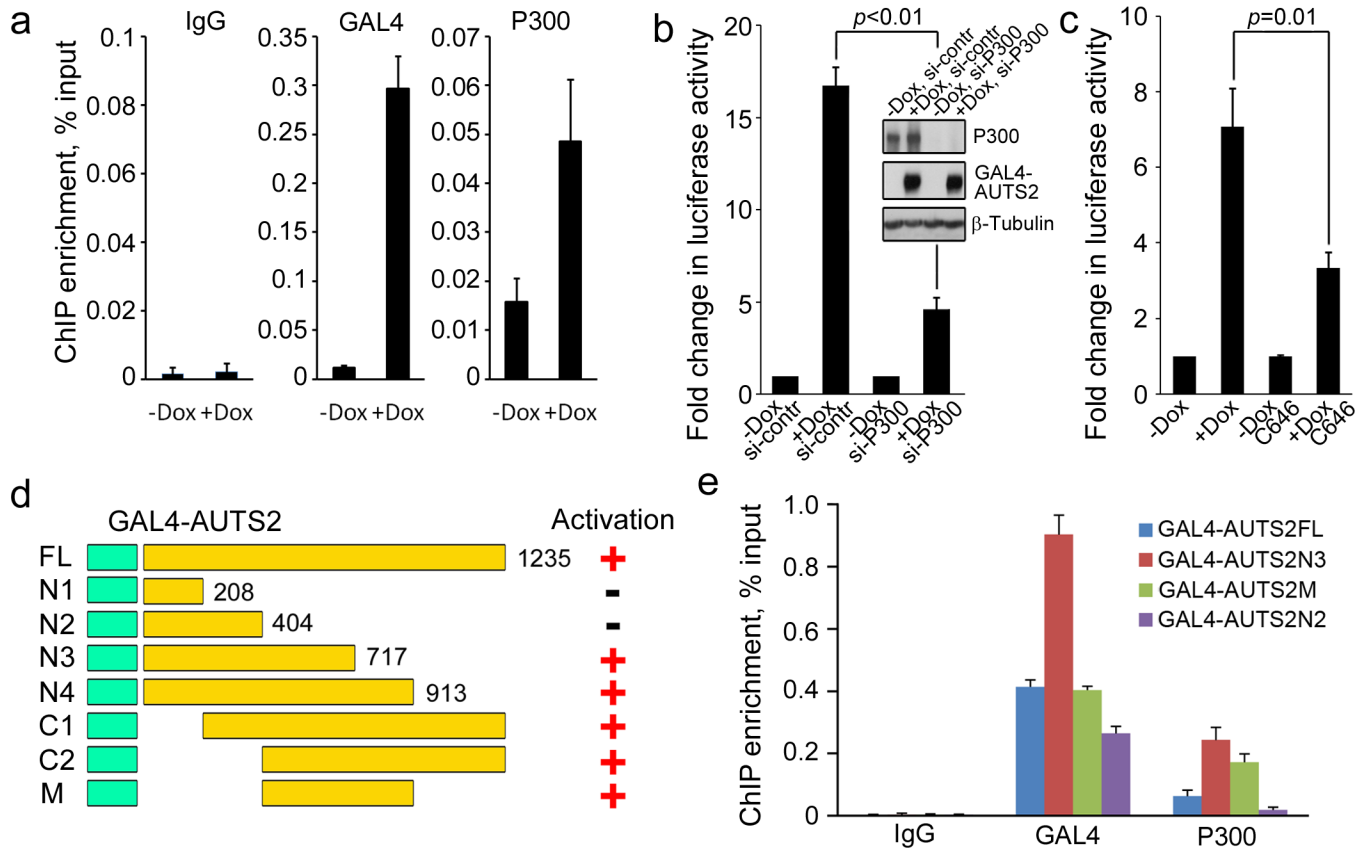
**Figure 4. AUTS2 recruits P300 for gene activation**

**a** ChIP analysis of P300 in GAl4-AUTS2 cells, before and after doxycycline induction, as indicated.

**b** Fold change in luciferase activity in GAl4-AUTS2 cells with control (si-contr) or P300 siRNA (si-P300) treatment for 48 hr prior to 24 hr doxycycline induction. Insert shows immunoblotting of samples used for luciferase reporter assays using the antibodies indicated. The *p* value derived from two-sided *t*-test is indicated here and in **c**.

**c** Fold change in luciferase activity in GAl4-AUTS2 cells with or without C646 (Sigma) for 16 hr prior to 24 hr doxycycline induction.

**d** Mapping of AUTS2 domains required for transcriptional activation. Shown are schematic representations of stably expressed, truncated versions of AUTS2 fused to GAL4 (left) and their ability to stimulate luciferase activity (right).

**e** ChIP in stable cell lines expressing the candidates shown in **d** and performed with antibodies against GAL4 and P300.

a



c



d



b



e
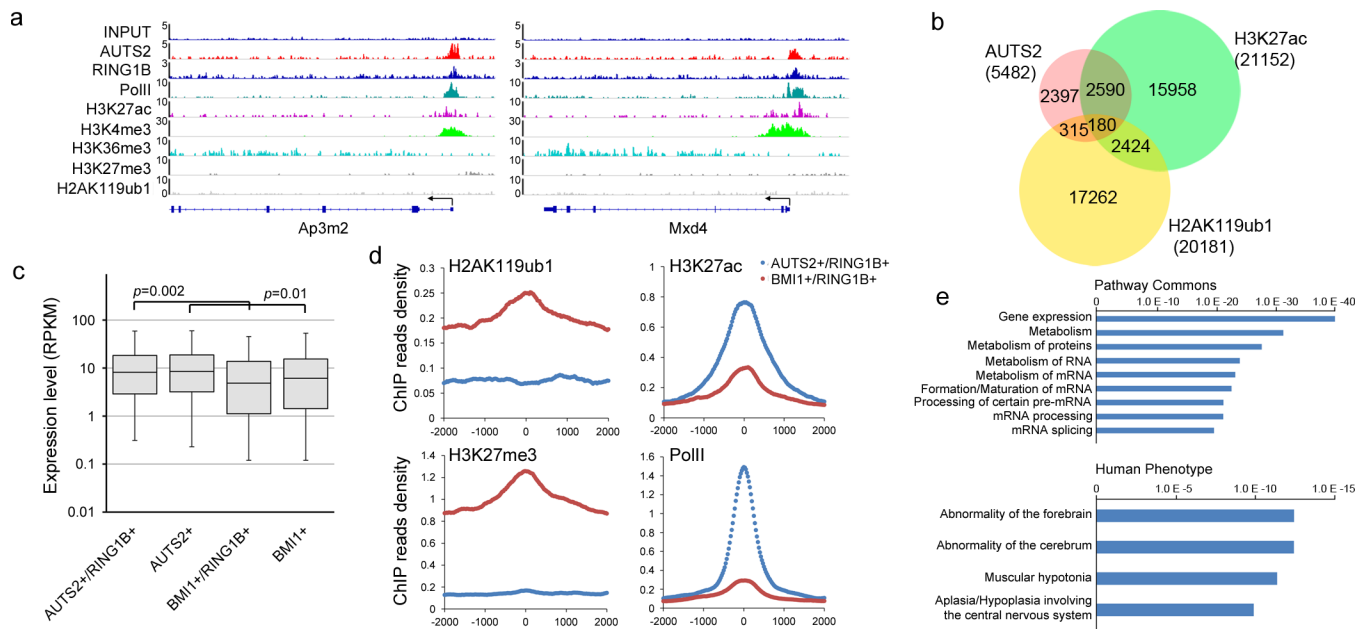


**Figure 5. Regulation of neuronal gene expression by AUTS2**

**a** IGV browser views for input, AUTS2, RING1B, Pol II, H3K27ac, H3K4me3, H3K36me3, H3K27me3, and H2AK119ub1. ChIP-seq performed in P1 mouse brain at two representative loci indicated. The y axis corresponds to ChIP-seq signal intensity.

**b** Venn diagram showing the overlap among target regions of AUTS2, H3K27ac, and H2AK119ub1.

**c** Expression analysis of genes targeted by AUTS2/RING1B, AUTS2 alone, BMI1/ RING1B, and BMI1 alone. RPKM (reads per kilobase of exon per million reads mapped) values are obtained from our RNA-seq data in mouse whole brain.

**d** ChIP reads density plots for levels of indicated histone marks and PolII at loci co-targeted by AUTS2/RING1B and BMI1/RING1B. A ±2 kb window relative to the center of peaks is shown. **e** GO analysis of targeted genomic regions identified by AUTS2 ChIP-seq, using GREAT. The x axis (in logarithmic scale) corresponds to the binomial raw $p$ values.
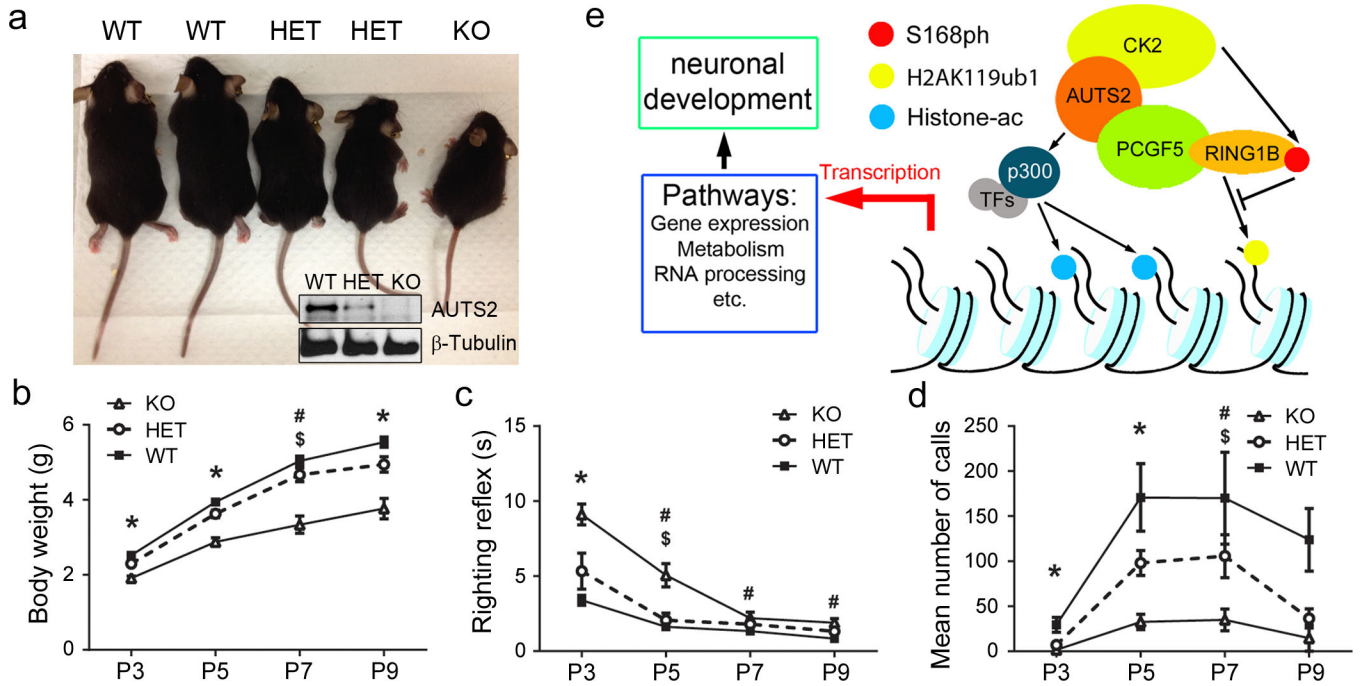
**Figure 6. Effect of *Auts2* KO on phenotypes associated with neurodevelopmental disorders**

**a** Comparison of the body size of WT, HET, and KO littermates. Insert shows immunoblotting of respective whole brain extracts.

**b** Both KO and HET mice weigh less than WT littermates across P3-P9. Data reported in all behavioral figure are mean and error bars are standard error of the mean. Post-hoc difference ($p < 0.05$) is indicated by * (between all three genotypes), # (between WT and KO), and $ (between HET and KO). Total numbers of mice used in the behavioral analyses are as following (the range reflects different numbers used for each behavioral test): at P3, WT 11–17, HET 3–10, KO 6–11; at P5, WT 23–27, HET 8–13, KO 18–19; at P7, WT 7–11, HET 3, KO 8; at P9, WT 4–8, HET 2–7, KO 3.

**c** KO mice show impairment in righting reflex relative to WT from P3-P9, while HET are not impaired.

**d** Both HET and KO mice show significantly less ultrasonic vocalizations (USVs) than WT following maternal separation across the majority of developmental time points measured.

**e** A model for PRC1.5-AUTS2-mediated transcriptional activation. See text for details.